WWW.OEAW.AC.AT

ÖAW ÖSTERREICHISCHE AKADEMIE DER WISSENSCHAFTEN

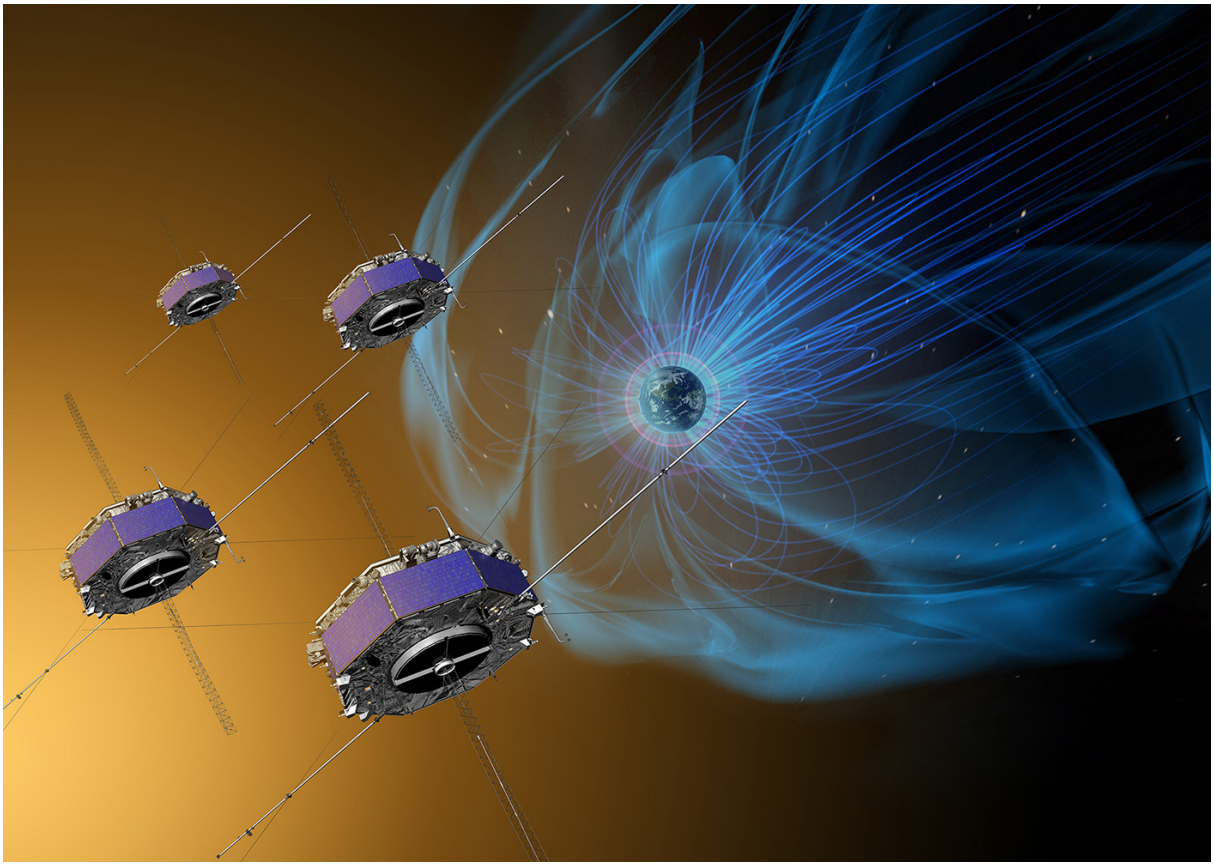

ANNUAL REPORT 2015

IWF INSTITUT FÜR WELTRAUMFORSCHUNG

IWF – INSTITUT FÜR WELTRAUMFORSCHUNG

ÖAW ÖSTERREICHISCHE AKADEMIE DER WISSENSCHAFTEN

ANNUAL REPORT 2015

IWF INSTITUT FÜR WELTRAUMFORSCHUNG

COVER IMAGE

NASA's *MMS* mission will solve the mystery of reconnecting magnetic fields around Earth (Credits: NASA).

TABLE OF CONTENTS

INTRODUCTION

The Space Research Institute (Institut für Weltraumforschung, IWF) in Graz has focused on the physics and exploration of the Solar System for over 40 years. With about 100 staff members from 20 nations it is one of the largest institutes of the Austrian Academy of Sciences (Österreichische Akademie der Wissenschaften, ÖAW).

IWF develops and builds space-qualified instruments and analyzes and interprets the data returned by them. Its core expertise is in building magnetometers and on-board computers, as well as in satellite laser ranging, which is performed at the IWF laser station Lustbühel. In terms of science, the institute concentrates on dynamical processes in space plasma physics, on the upper atmospheres of planets and exoplanets, and on the gravity fields of the Earth and Moon.

IWF cooperates closely with space agencies all over the world and with numerous other national and international research institutions. A particularly intense cooperation exists with the European Space Agency (ESA).

The institute is currently involved in eighteen active and future international space missions:

- *BepiColombo* will be launched in 2018 to investigate planet Mercury, using two orbiters, one specialized in magnetospheric studies and one in remote sensing.
- *Cassini* will continue to explore Saturn's magnetosphere and its moons until 2017.
- ESA's first S-class mission *CHEOPS (CHaracterizing ExOPlanets Satellite)* will classify exoplanets in detail. Its launch is expected in 2018.
- The *China Seismo-Electromagnetic Satellite (CSES)* will be launched in 2016 to study the Earth's ionosphere.
- The *Chinese Mars Mission* is scheduled for launch in 2022.
- *Cluster*, ESA's four-spacecraft mission, is still providing unique data leading to a new understanding of space plasmas.
- *GEO-KOMPSAT-2A* is a Korean satellite for space weather investigations due for launch in 2018.

Fig. 1: An Atlas V rocket carrying the MMS payload for NASA lifted off from Cape Canaveral Air Force Station in Florida at 10:44 p.m. EDT on 12 March 2015 (Credits: United Launch Alliance).

- *InSight (INterior exploration using Seismic Investigations, Geodesy and Heat Transport)* is a NASA Discovery Program mission that will place a single geophysical lander on Mars to study its deep interior. It is expected for launch not earlier than 2018.
- ESA's *JUpiter ICy moons Explorer (JUICE)* will observe the giant gaseous planet Jupiter and three of its largest moons, Ganymede, Callisto, and Europa. It is planned for launch in 2022.
- *Juno* is a NASA mission dedicated to understand Jupiter's origin and evolution. It is slated to arrive at the gas giant planet on 4 July 2016.
- *MMS*, successfully launched in March 2015 (Fig. 1), is using four identically equipped spacecraft to explore the acceleration processes that govern the dynamics of the Earth's magnetosphere and has delivered promising early results.
- ESA's third Medium-class science mission *PLATO* is a space-based observatory to search for planets orbiting alien stars. It is planned for launch by 2024.
- *Resonance* is a Russian space mission of four identical spacecraft, orbiting partially within the same magnetic flux tube, scheduled for launch in 2018.
- *Rosetta* finished its main mission in December 2015 and received an extension until September 2016.
- *Solar Orbiter* is to study along an innovative trajectory solar and heliospheric phenomena, planned for launch in 2018.
- *STEREO* studies solar (wind) structures with two spacecraft orbiting the Sun approximately at Earth's distance.
- *THEMIS* has been reduced to a near-Earth three-spacecraft mission. The two other spacecraft are now orbiting the Moon in the *ARTEMIS* mission.
- The *Van Allen Probes* are two NASA spacecraft, studying the dynamics of the Earth's radiation belts.

HIGHLIGHTS IN 2015

- On 12 March 2015 (US local time), NASA's *Magnetospheric Multi-Scale (MMS)* mission successfully launched to explore the dynamics of the Earth's magnetosphere and its underlying energy transfer processes. IWF, as biggest non-US partner in *MMS*, has taken the lead for the spacecraft potential control of the satellites and is participating in the electron beam instrument and the digital fluxgate magnetometer.
- The first results of the *Rosetta/Philae* mission have been published in „Science" with co-authors from IWF. Three papers describe the landing trajectory and show that the nucleus of comet 67P/Churyumov-Gerasimenko is not magnetized and that its surface is covered by a -160 °C cold and unexpectedly solid layer.
- In order to better predict solar storms, data of seven spacecraft have been used, which investigate the solar corona, the solar wind, and even the radiation on the Martian surface, measured by the *Curiosity Rover*.
- For the first time, the secondary soft X-ray emission for close-in exoplanets was estimated, which is produced due to charge-exchange of heavy stellar wind ions with the neutral atmospheric particles. It was found that the emissions for a typical hot Jupiter are a million times stronger than the emission from the Jovian aurora.

THE YEAR 2015 IN NUMBERS

Members of the institute published 126 papers in refereed international journals, of which 34 were first author publications. During the same period, articles with authors from the institute were cited 3760 times in the international literature. In addition, 89 talks and 51 posters have been presented at international conferences by members of the IWF, including 21 by special invitation from the conveners. Last but not least, institute members organized and chaired 18 sessions at 7 international meetings.

IWF STRUCTURE AND FUNDING

IWF was, as a heritage since foundation, structured into three departments. Nowadays, the institute has been restructured into four research fields consisting of nine working groups (Fig. 2). Wolfgang Baumjohann serves as Director, Werner Magnes as Deputy Director.

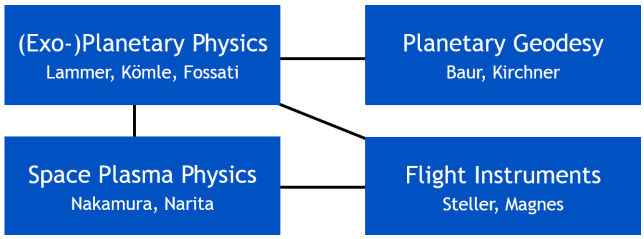

Fig. 2: IWF research fields and group leaders.

The bulk of financial support is provided by ÖAW. Significant support is also given by other national institutions, in particular the Austrian Research Promotion Agency (Österreichische Forschungsförderungsgesellschaft, FFG) and the Austrian Science Fund (Fonds zur Förderung der wissenschaftlichen Forschung, FWF). Furthermore, European institutions like ESA and the European Union contribute substantially.

EARTH & MOON

Gravimetric and geometric space geodesy techniques constitute an integral part in Earth and planetary sciences. In order to improve our knowledge about the environment, state and evolution of the Earth and the Earth's only natural satellite, the Moon, IWF is engaged in terrestrial and lunar gravity field research, selected studies of the Earth's atmosphere and crustal dynamics, and Satellite Laser Ranging (SLR) to Earth-orbiting spacecraft and debris objects.

GRAVITY FIELD

Gravity field research includes the analysis of data collected by Earth- and Moon-orbiting spacecraft and SLR to passive satellites.

GRACE FOLLOW-ON

In the last decade, mass change quantification from data collected by the *GRACE (Gravity Recovery And Climate Experiment)* gravity field mission advanced to a key source of information in climate research. Today, owing to improved data processing, the gravity-based inference of surface mass change is no longer limited to the Greenland and Antarctica ice sheets, but glacier systems attract increasing attention. With the *GRACE Follow-On* mission (Fig. 3), due for launch in late 2017, a further step towards small-scale mass variation quantification can be expected.

Fig. 3: Artist's view of the *GRACE Follow-On* mission (Credits: GFO satellites: AEI/Daniel Schütze, Background: NASA/NOAA/GSFC/ SuomiNPP/VIIRS/Norman Kuring).

GOCO

The main objective of the *Gravity Observations COmbination (GOCO)* consortium, an Austrian-German-Swiss initiative, is to compute high-accuracy and high-resolution global gravity field models from complementary gravity data sources. Within this initiative, IWF is responsible for the Satellite Laser Ranging (SLR) component. SLR is a powerful technique for the estimation of the very long wavelengths components of the Earth's gravity field. The most important parameter in this context is C20 - it represents the Earth's dynamic flattening, which is responsible for the largest deviation of the real figure of the Earth from its spherical approximation. Despite of having data available from a number of dedicated gravity field missions such as *GRACE* and *GOCE*, SLR is still superior for the determination of C20, but the technique also significantly contributes to the recovery of further low-degree gravity field parameters (Fig. 4). The latest satellite-only gravity field model within the GOCO series (GOCO05S) was released in 2015. The SLR part was set up from measurements to six geodetic satellites.

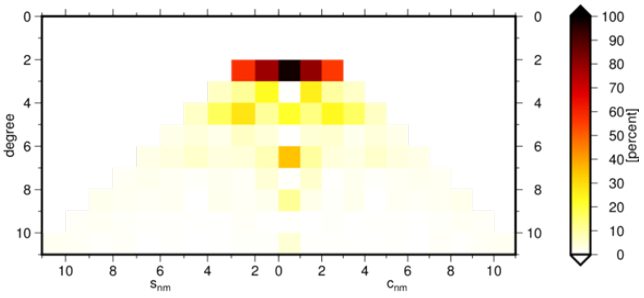

Fig. 4: Contribution of SLR to the gravity field model GOCO05S. The contribution is largest for the degree-2 spherical harmonic coefficients; C20 can be considered to be reconstructed from purely SLR.

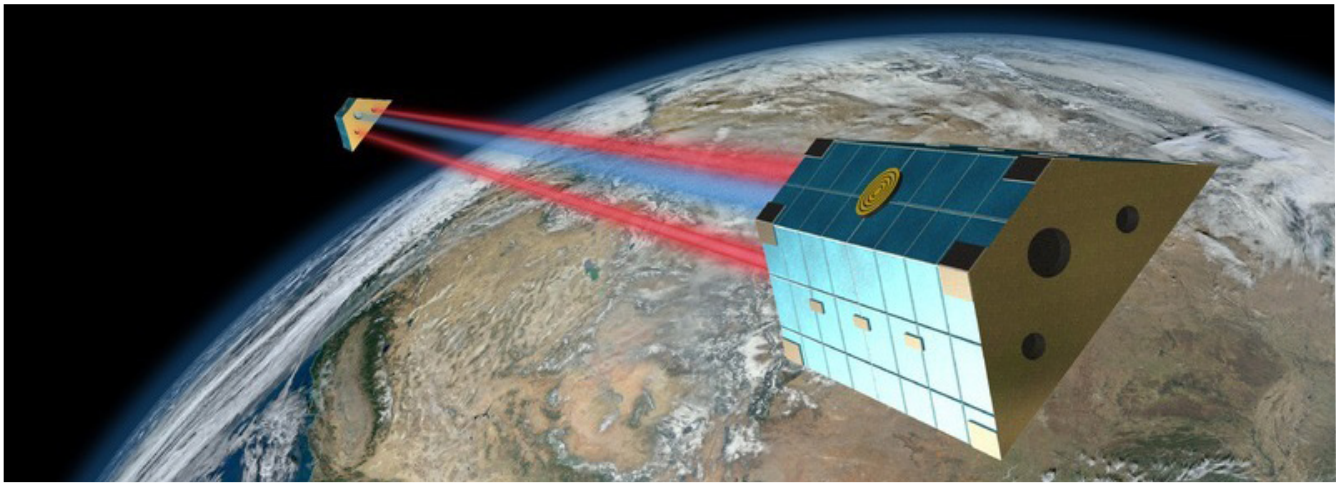

GRAIL

The *Gravity Recovery And Interior Laboratory (GRAIL)* mission launched by NASA on 10 September 2011, eclipses any previous attempt to recover detailed gravitational features of the Moon. The mission consists of two identical spacecraft following each other in a low-altitude (~55 km), near-circular and near-polar orbit. In order to reconstruct the lunar gravity field the mission performs Ka-band range-rate measurements between the two satellites, thus allowing continuous data acquisition on the nearside and the farside of the Moon. To analyze these observations a short-arc integral approach based on the reformulation of Newton's equation of motion as a boundary problem is adopted. Gravitational forces (third-body attractions, tides, general relativistic effects) and non-gravitational forces (solar radiation pressure, lunar albedo and emissivity) are properly taken into account.

In addition to the estimation of a time bias (1/day) and empirical accelerations (2/rev) the latest Graz Lunar Gravity Models (GrazLGM) consider a priori information in terms of co-variance functions. Fig. 5 shows a free-air gravity anomaly map derived from the GrazLGM300b model, revealing numerous craters on the nearside and farside of the Moon. Owing to extensive performance tests in the framework of a Partnership for Advanced Computing in Europe (PRACE) preparatory access project, the analysis software has been prepared for High Performance Computing (HPC) environments, and hence IWF in-house HPC architecture.

GEODYNAMICS

Presently, there are four Global Navigation Satellite Systems (GNSS) designed for a wide range of civil and military purposes: GPS (USA), GLONASS (Russia), Beidou (China), and GALILEO (European Union). Transmitting data within the 1-2 GHz frequency range, the scientific goal is to use them for investigating physical processes of the ionosphere, the troposphere, and the Earth's crust. Most importantly, the receiving permanent stations are the basis for any global geometric reference. Whereas navigation tasks can easily be tackled by handheld receivers with a precision of a few meters in real time (may improve to decimeters in the near future), reference frame maintenance poses millimeter precision requirements. The arguments for using more than one GNSS (referred to as multi-GNSS) is less the advantage of having more satellites available under difficult topographic conditions, but to get performance advantages by combining more signals with different frequencies. This is most obvious for the ionosphere, which is a dispersive medium for microwave signals. The major disadvantage of the multi-GNSS concept is the handling of biases between the individual systems (e.g., antenna positon variations due to different handling of solar panel movements). For this reason, a new Receiver INdependent EX-change (RINEX) format has been developed. Data centers are asked to make multi-GNSS data available. As one of the first data centers worldwide, the Lustbühel Observatory realized this task in 2015. A GPS+GLONASS combination is running daily, which helps to substantially improve resolving the behavior of the Earth's crust and climate troposphere parameters. Lustbühel Observatory also contributes to the global project REPRO2, which aims at the homogenization of 20 years of GNSS results – mainly in the context of climate and geodynamic research. Concerning the latter, the estimation of local elastic parameters related to earthquakes is of particular interest.

Fig. 5: Root mean square (RMS) values per spherical harmonic degree. Black graph: GLw0660 signal; color graphs: differences to GL0660.

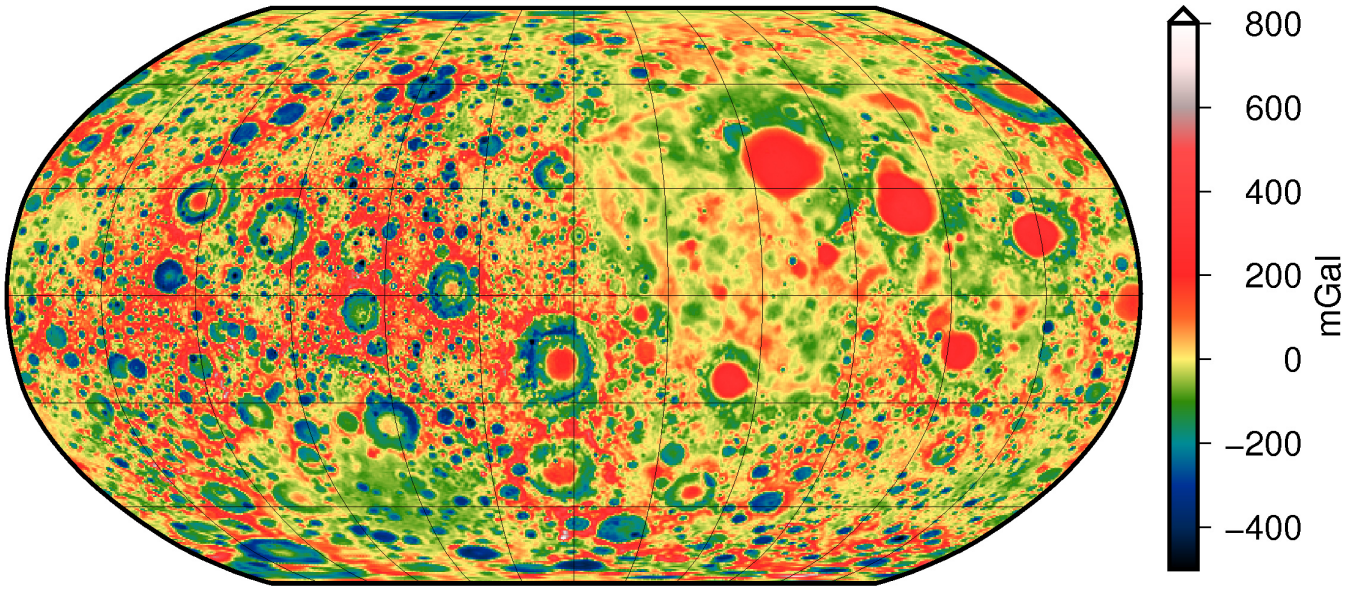

ATMOSPHERE

For the period July 2003 to August 2010, the Coronal Mass Ejection (CME) catalogue maintained by Richardson and Cane lists more than 100 Earth-directed events. These events have been sensed in-situ by plasma and field instruments on board of the Advanced Composite Explorer (ACE) satellite located at Lagrange point L1 upstream of the Earth. Since the majority of CMEs causes a distinct density enhancement of the Earth's thermosphere, a statistical study based on accelerometer measurements from the low-Earth orbiting GRACE satellite mission was carried out.

Correlations between neutral density variations and CME parameters (magnetic field component Bz, maximum CME velocity, etc.) as well as several geomagnetic indices were evaluated. The highest correlation coefficient (cc) was determined between density increase and the Bz component (cc=-0.92); Fig. 6 shows a latitude-time plot of these two quantities. As far as geomagnetic indices are concerned, the Disturbance Storm Time (Dst) index (cc=-0.91) and the AM index (cc=0.92) show highest correlation with density increase. The correlation is less pronounced for the Kp index and the auroral electrojet.

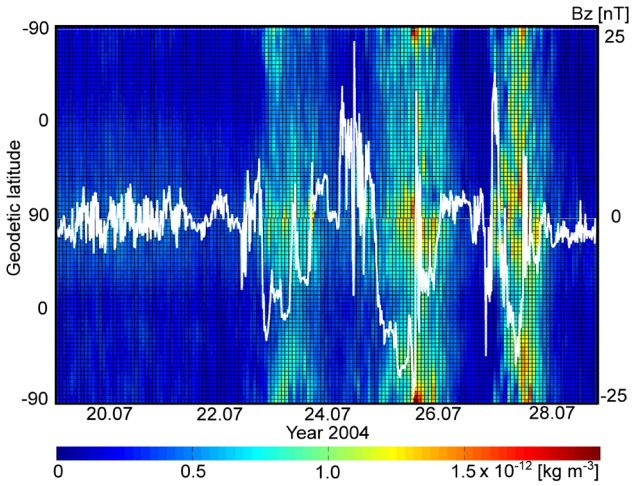

Fig. 6: Latitude-time plot of thermospheric densities derived from *GRACE* accelerometry. The impact of three CMEs in July 2004 inducing severe geomagnetic storms can be identified in the density increase and the magnetic field measurements observed by ACE (white line).

SATELLITE LASER RANGING

The still ongoing routine tracking of satellites equipped with laser retro-reflectors (143 satellites) was again the basis for several research activities. Most of the scientific achievements and results take advantage of the highly accurate Graz kHz SLR system. For space debris attitude motion determination, laser measurements can now be combined with simultaneously observed light curves.

Single Photon DART, Nano-DART, Pico-DART: The development of the Single-Photon Detection, Alignment and Reference Tool (SP-DART) was finalized. To establish a reference, the SP-DART system was installed at the Graz SLR station, measuring with both the Graz laser and the DART laser system in parallel. In this setup, the SP-DART laser transmitter (Fig. 7) was mounted at the SLR telescope. All necessary equipment was installed (FPGA range rate generator, event timer, GPS timing system, meteorology measurement devices, etc.). Using this setup, measurements to Earth-orbiting satellites up to Global Navigation Satellite System (GNSS) altitude (~20000 km) have been performed successfully.

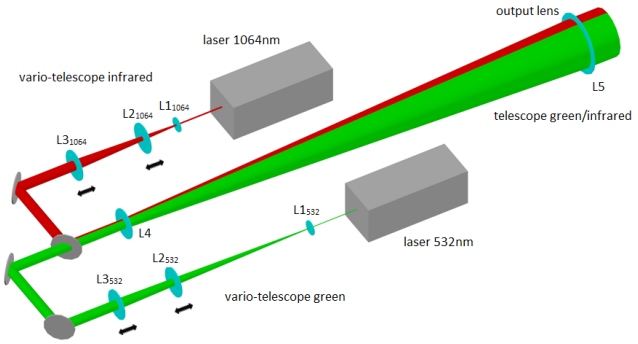

Fig. 7: Principal design of the SP-DART laser transmitter. Both beams at exit 40 mm diameter, minimum divergence <25 μrad; both lasers operating in parallel, no moving parts, pointing stability <15 μrad.

The SP-DART basically is a small SLR station, using a host telescope. Combined with a standard astronomical telescope and a suitable mount – and with a single-photon detector installed – it can be considered as a fully operational SLR station. Different versions are planned for the future: using a picosecond laser (referred to as pico-DART) for high accuracy applications once such a laser with suitable parameters becomes available, or using the already available nanosecond laser (nano-DART) for SLR to GNSS retro-reflector panels. These realizations may be combined with autonomous / automatized SLR operation.

Single-Photon DART on tour: In order to demonstrate the feasibility of the SP-DART as a „checking tool" for single-photon sensitivity of other SLR stations, the equipment was installed at SLR station Wettzell for testing purposes (Fig. 8). After aligning the SP-DART laser beam parallel to the Wettzell laser beam – which turned out to be far from trivial – again distances up to GNSS altitude could be measured. The return quotes from GNSS satellites were similar to those measured in Graz (as an example, for GLONASS 128 the return rate was approx. 3%, corresponding to about 60 returns/sec with 15 µJ/pulse), proving that both receiver systems (Graz and Wettzell) achieve similar single-photon sensitivity. In 2016, further SLR stations – but also astronomical sites – are supposed to be visited in order to investigate their single-photon sensitivity.

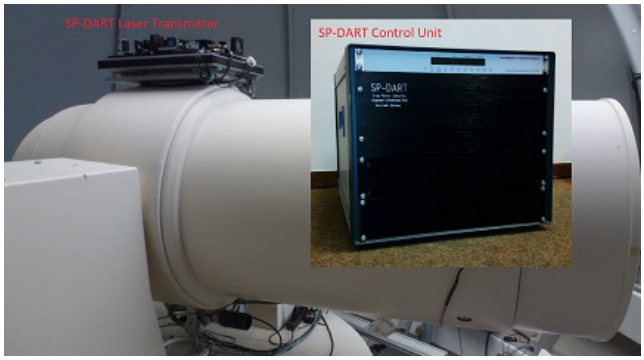

Fig. 8: SP-DART laser transmitting part mounted on the Wettzell SLR telescope.

Space debris orbit prediction: Since decades, SLR contributes to precise orbit determination and orbit prediction of geodetic satellites and operational spacecraft. Apart from this routine task, SLR has the potential to significantly improve orbit predictions of (selected) space debris objects, and hence to substantially contribute to Space Situational Awareness tasks. Orbit predictions – in terms of Two Line Elements (TLEs) – of the Joint Space Operation Center suffer accuracy and reliability. Against this background, a Space Debris Data Information System (SDDIS) based on SLR data has been established at IWF. Currently, the SDDIS gathers and disseminates tracking data and orbit predictions of about 30 space debris objects. Most of these objects are abandoned satellites in the highly-populated low-Earth orbit segment. This segment is of utmost interest for any space faring nation.

As an example, Fig. 9 demonstrates the benefit of SLR for precise orbit determination/prediction. A posteriori laser tracking residuals to Topex/Poseidon reveal the superiority of laser-based orbit predictions over TLEs by about two orders of magnitude. This allows not only for daytime tracking, but also for accurate attitude and spin determination.

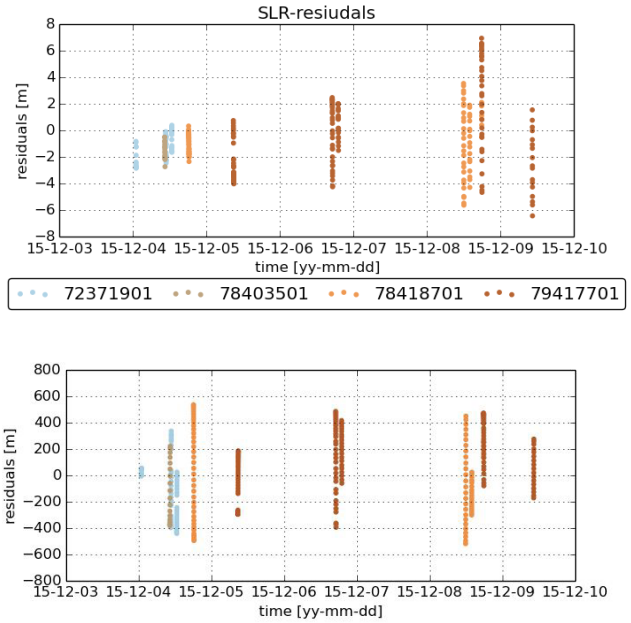

Fig. 9: A posteriori SLR residuals of Topex/Poseidon. Top: laser-derived orbit prediction; bottom: TLE-based orbit prediction. Different scales apply.

Spin determination via light curves: For the time being, the standard method to determine satellite spin periods is based on the periodicity of laser retro-reflector echoes. In addition, a second method was implemented utilizing light curve analysis: a dichroic mirror separates light, which is reflected by the satellite. Light between 780 nm and 900 nm – which is not used for standard SLR detection – is passed to four additional single-photon detection and counting units. Each detector is sensitive to a different polarization state, which is a requirement for future quantum cryptography experiments. All detectors are operating in a free running mode (prepared for a fifth detector sensitive in the infrared spectral range). A powerful FPGA board collects the single events, giving them a timestamp and transfers the data to a Brick-PC for storage (Fig. 10).

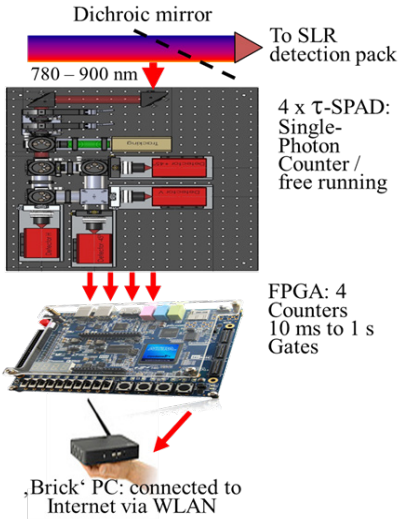

Fig. 10: Light curve measurement unit mounted on Graz SLR telescope.

The data are collected – independently from and simultaneously with SLR operation – for a wide range of satellites in low to high orbital altitude. Mean light curves (Fig. 11) are eventually obtained by utilizing the phase dispersion minimization algorithm.

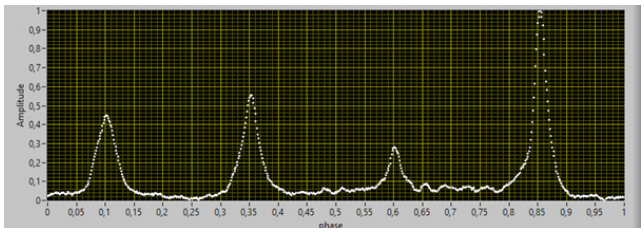

Fig. 11: Light curve of the Compass G2 satellite. One phase interval (x-axis) corresponds to a spin period of 7.14 s.

One of the big advantages of this method compared to alternative techniques lies in the independence of the measurements from the "visibility" of retro-reflectors, as the detected signal is sunlight reflected from the whole satellite. In total, the spin periods of more than 40 GLONASS satellites have been determined by one or by both of the mentioned methods (Fig. 12), with the benefit that ambiguities can be resolved easily. The spin periods determined via light curve analysis show excellent agreement with SLR results. The intensity curves of the reflected light allow drawing conclusions on the orientation of the satellites relative to the observer. For the Compass G2 satellite, as an example, two reflection peaks intensify within a few hundred seconds. This is the case when the observing direction coincides with the intensity maximum of the diffuse reflection of a satellite surface.

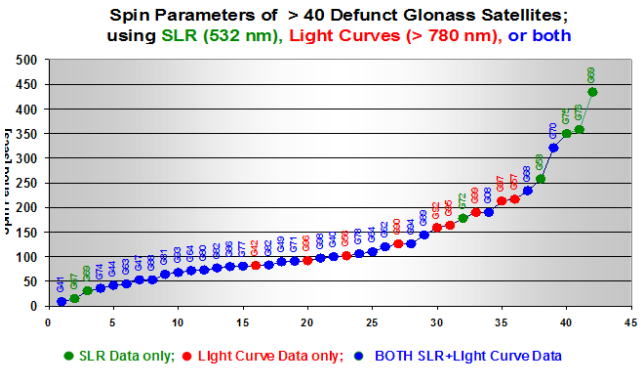

Fig. 12: Spin periods (in seconds) of various GLONASS satellites measured with SLR (green), light curves (red), or both (blue).

Space debris real-time pointing determination by wide-angle image analysis: Laser ranging to space debris often suffers from inaccurate orbit prediction. This can be improved by the so-called "stare and chase" method. An astronomical imaging camera with high sensitivity is combined with a common photo-objective of low focal length to generate a wide field of view of about ten degrees. The camera records the stellar background with a 25 Hz frame rate by "staring" in an approximate direction where the debris is expected. As soon as the debris – illuminated by sunlight – enters the field of view, software determines the pixel values of the object on the chip (Fig. 13). Simultaneously, by analyzing the stellar background with a plate solving algorithm, the pointing information to the passing satellite is recorded in equatorial coordinates.

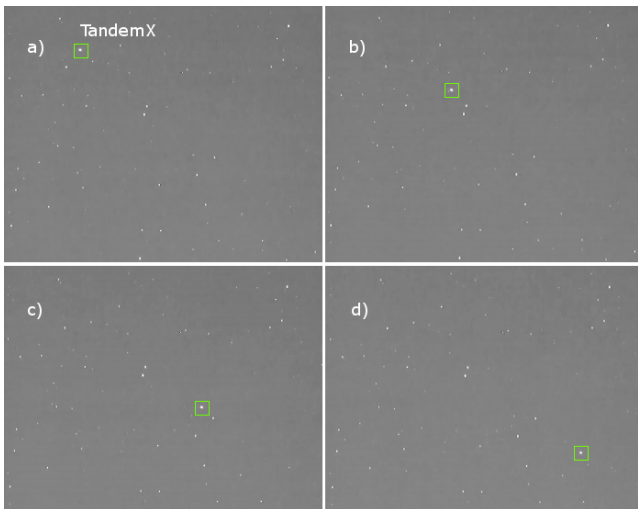

Fig. 13: Tandem-X satellite passing through the field of view (a-d) being identified by automatized software while recording the pointing information.

The idea is to use this pointing information to calculate more accurate orbit predictions for the remaining part of the pass – or for the next pass – of the satellite, thus allowing to conduct SLR measurements to this target ("chase"), which in turn improves orbit prediction accuracy.

NEAR-EARTH SPACE

Near-Earth space is an ideal environment to study fundamental plasma processes based on in-situ measurements of the charged particles together with electric and magnetic fields. IWF is participating in the hardware activities of numerous spacecraft missions, now operating, being built or planned. Based on different analysis methods supported by theoretical models, the data taken from these missions have been extensively analyzed and new physical knowledge is obtained.

CLUSTER

The *Cluster* spacecraft have been providing data since 2001 for studying small-scale structures of the magnetosphere and its environment as the first four spacecraft mission in space. IWF is PI/Co-I on five instruments and maintained the Austrian Data Centre. All data are archived in *Cluster* Science Archives (CSA) including supporting data products such as science event lists and ground-based data. The mission is planned to be extended to December 2018.

THEMIS/ARTEMIS

NASA's *THEMIS* mission, launched in 2007, consisted of five identical satellites flying through different regions of the magnetosphere. In autumn 2010 the two outer spacecraft became *ARTEMIS*, while the other three *THEMIS* spacecraft remained in their orbit. As Co-I of the magnetometer, IWF is participating in processing and analyzing data.

MMS

NASA's *MMS* mission (Magnetospheric Multiscale) explores the dynamics of the Earth's magnetosphere and its underlying energy transfer processes. Four identically equipped spacecraft carry out three-dimensional measurements in the Earth's magnetosphere. *MMS* investigates the small-scale basic plasma processes, which transport, accelerate and energize plasmas in thin boundary and current layers. IWF, which is the biggest non-US participant in *MMS*, has taken the lead for the spacecraft potential control *(ASPOC)* and is participating in the electron beam instrument *(EDI)* and the digital fluxgate magnetometer *(DFG)*. *MMS* was launched on 12 March 2015 at 10:44 pm US local time (Fig. 15). Until the end of August, all spacecraft were successfully commissioned, followed by the official start of the first scientific phase on 1 September 2015.

Fig. 14: Launch of the four MMS spacecraft with an Atlas V rocket from Kennedy Space Center (Credits: Ben Cooper, launchphotography.com).

Active Spacecraft Potential Control (ASPOC) instrument: *ASPOC* neutralizes the spacecraft potential by releasing positive charged indium and thereby controlling the spacecraft potential. This enables accurate measurements also in sparse plasma environments essential to study properties of reconnection, which is the main scientific goal of *MMS*.

After launch, *ASPOC* participated in the commissioning campaign, which consisted of nine different activities including low/high voltage tests and cross-instrument checkouts. It has been shown already in early commissioning phase that *ASPOC* controls the spacecraft potential below 4 V in consistence with the science requirement of *MMS*. Since the completion of the commissioning activities in July, all *ASPOC* units are operating in nominal mode without any problems and are participating in the science phase activities as shown in Fig. 15. The *ASPOC* level 1/2 science data products are processed on a daily basis and are immediately available from the Science Data Center at LASP/Colorado.

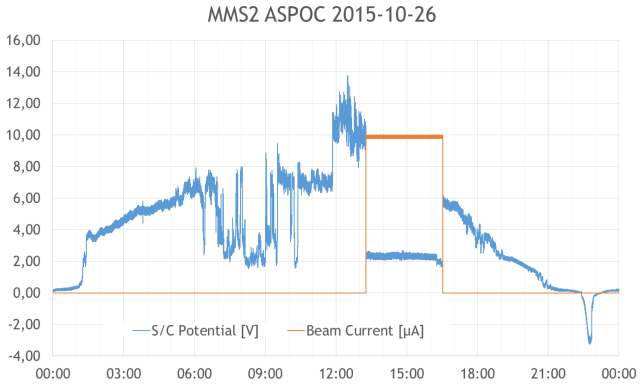

Fig. 15: *ASPOC* ion beam current (orange) and spacecraft potential (blue) during one orbit. It can be seen that the spacecraft potential is kept to a near-constant level of about 2 V when *ASPOC* is operating.

Electron Drift Instrument (EDI): IWF contributed to *EDI* with the *Gun Detector Electronics (GDE)* and the electron gun. The *GDE* was developed by Austrian industry in close cooperation with the institute, while the electron gun was entirely developed by IWF.

EDI is based on the *Cluster* development with several improvements. Because of the use of high voltage, the *EDI* instrument has been switched on a few weeks after launch, to avoid discharges due to residual gas in the instrument. The operation is changed to reduce the stress to the sensitive high voltage optocoupler, thus optimizing the instrument's lifetime. The 500 eV energy mode has become the preferred operation mode. The 1 keV beam energy is used only if required by the plasma conditions.

A statistic over the first month of operation shows good quality of the returns (Fig. 16). In the perpendicular direction the entire polar angle of 95° can be used. In the parallel direction a portion of the high angle region is shadowed by neighboring instruments.

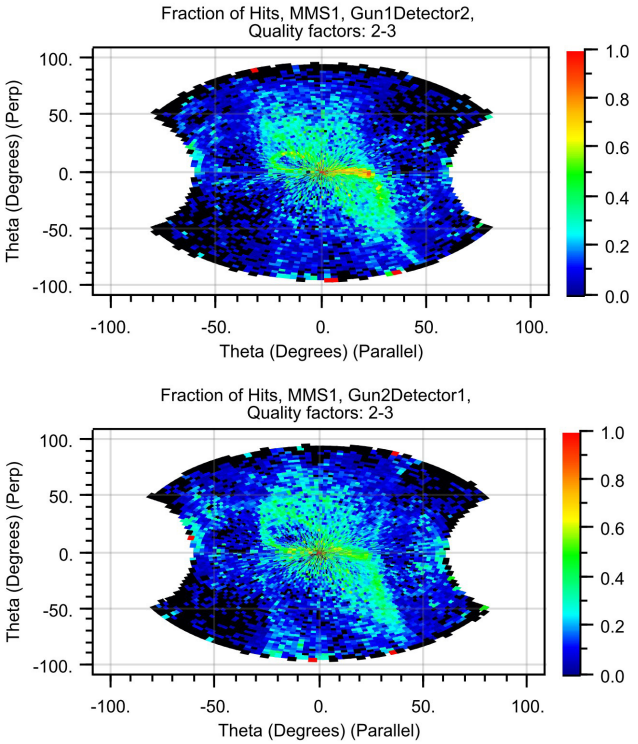

Fig. 16: Statistics of beam returns for the instrument aboard *MMS1* (Credits: UI/Scott Bourns).

Digital FluxGate magnetometer (DFG): *DFG* is based on a triaxial fluxgate magnetometer developed by the University of California, Los Angeles, and a front-end Application Specific Integrated Circuit (ASIC) for magnetic field sensors. The ASIC has been developed by IWF in cooperation with the Fraunhofer Institute for Integrated Circuits.

Until launch, IWF contributed to the system level testing of the *DFG* instruments with the careful evaluation of comprehensive test data acquired from the *DFGs* by the *FIELDS* central processing unit. During commissioning phase, IWF supervised the first power-on of the four *DFG* magnetometers as well as the boom deployments. It was followed by the comparison of the calibration parameters obtained in-flight with those measured before launch. It turned out that they match very well.

Spin axis offset calibration and combined data product: Methods for determining spin axis offset of the fluxgate magnetometers *AFG* and *DFG* using absolute magnetic field values deduced from *EDI* could be further improved. From August 2015 it was possible to apply the time-of-flight (TOF) method successfully and to constrain the spin axis offsets. This has improved the absolute accuracy of *AFG* and *DFG* to better than 0.2 nT. By themselves, search coil and fluxgate magnetometers cannot provide the best possible signal-to-noise ratio. Thus, it is beneficial to combine data sets from both instruments for advanced scientific analysis. Based on *MMS* flight data, a refinement of the combination model took place, an adaptation of the combination software could be finished, and regular processing of burst data has been started.

CSES

The *China Seismo-Electromagnetic Satellite (CSES)* is scheduled for launch at the end of 2016 and will be the first Chinese platform for the investigation of natural electromagnetic phenomena with major emphasis on earthquake monitoring from a Sun synchronous, polar, Low Earth Orbit. The *CSES* magnetometer is developed in cooperation between the National Space Science Center (NSSC) of the Chinese Academy of Sciences, IWF, and the Institute of Experimental Physics of the Graz University of Technology (TUG). NSSC is responsible for the dual sensor fluxgate magnetometer, the instrument processor, and the power supply unit. IWF and TUG participate with the newly developed absolute scalar magnetometer, called *Coupled Dark State Magnetometer (CDSM)*. In 2015, the *CDSM* Qualification Model (Fig. 17) was delivered to China and the qualification tests have been successfully finished.

Fig. 17: CDSM Qualification Model with sensor, optical fibers and electronics unit (from left to right).

GEO-KOMPSAT-2A

A prototype of a *Service Oriented Spacecraft MAGnetometer (SOSMAG)* is being developed for ESA's Space Situational Awareness program, which shall serve as a ready-to-use space weather monitoring system to be mounted on a variety of different spacecraft built without a magnetic cleanliness program. Up to two high resolution boom-mounted fluxgate-magnetometers, the Digital Processing Unit (DPU) and the boom are provided by Magson GmbH and the Technical University of Braunschweig. For detection and characterization of magnetic disturbers on the spacecraft, two magnetometers based on the anisotropic magnetoresistive (AMR) effect were developed in a joint effort by Imperial College London and IWF. In 2015, the electronics design has been updated so that *SOSMAG* can be used for space weather research aboard the South Korean *GEO-KOMPSAT-2A* mission as part of the *Korean Space Environment Monitor (KSEM)* instrument suit. It will be launched into a geostationary orbit in May 2018.

PHYSICS

Various data from ongoing missions are analyzed and theoretical models are developed to describe the physical processes in near-Earth space. The studies deal with interactions between solar wind and magnetosphere, internal disturbances in the magnetosphere such as plasma flows and waves, and plasma instabilities including magnetic reconnection.

Frequencies of standing magnetopause surface waves: It has been proposed that the subsolar magnetopause may support its own eigenmode, consisting of propagating surface waves which reflect at the northern/southern ionospheres forming a standing wave. While the eigenfrequencies of these so-called Kruskal-Schwarzschild (KS) modes have been estimated under typical conditions, the potential distribution of frequencies over the full range of solar wind conditions has been unknown.

Using models of the magnetosphere and magnetosheath applied to an entire solar cycle's solar wind data, time-of-flight calculations yielding a database of KS mode frequencies have been performed. Under non-storm times or northward interplanetary magnetic field (IMF), the most likely fundamental frequency is calculated to be 0.64 mHz, consistent with previous estimates and indirect observational evidence for KS modes. However, the distributions exhibit significant spread (Fig. 18) demonstrating that KS mode frequencies, especially higher harmonics, should vary considerably depending on the solar wind conditions.

The subsolar magnetopause eigenfrequencies are found to be most dependent on the solar wind speed, southward component of the IMF, and the Dst index, with the latter two being due to the erosion of the magnetosphere by reconnection. Furthermore, the possible occurrence of KS modes is shown to be strongly controlled by the dipole tilt angle.

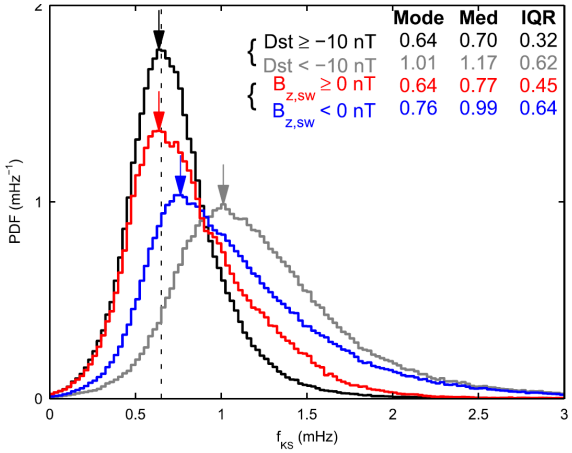

Fig. 18: Distributions of fundamental KS mode frequencies for different conditions. Most likely frequencies as well as median frequencies and interquartile ranges of the distributions are indicated.

Anharmonic oscillatory flow braking in the Earth's magnetotail: Plasma sheet bursty bulk flows often oscillate around their equilibrium position at about 10 RE downtail. The radial magnetic field, pressure, and flux tube volume profiles usually behave differently earthward and tailward of this position. Using data from five *THEMIS* probes, the profiles were reconstructed with the help of an empirical model and application of thin filament theory to show that the oscillatory flow braking can occur in an asymmetric potential. Thus, the thin filament oscillations, shown in Fig. 19, appear to be anharmonic, with a power spectrum exhibiting peaks at both the fundamental frequency and the first harmonic. Such anharmonic oscillatory braking can explain the presence of the first harmonic in Pi2 pulsations (frequency doubling), which are simultaneously observed by magnetometers on the ground near the conjugate *THEMIS* footprint.

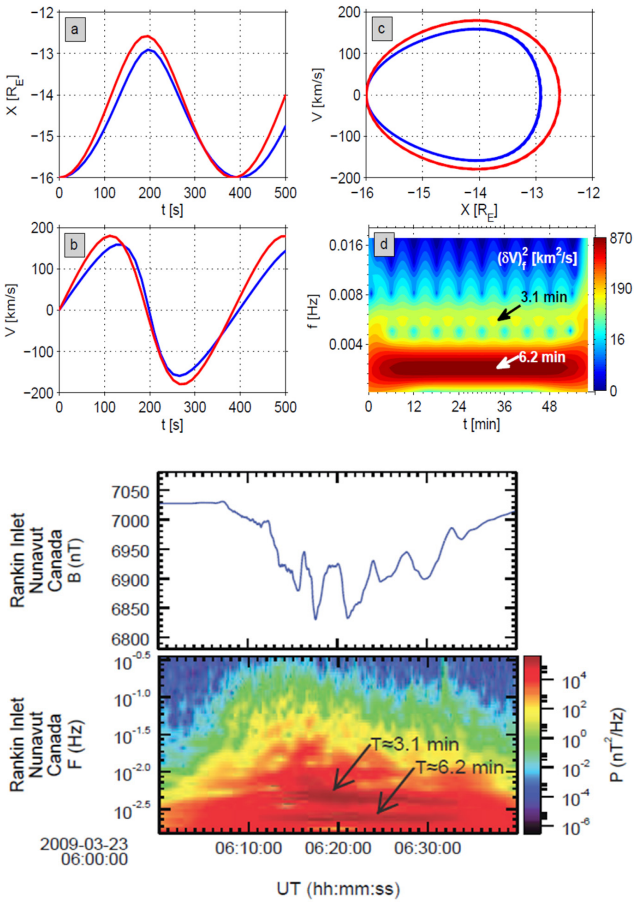

Fig. 19: Anharmonic thin filament oscillation in an asymmetric potential around the equilibrium position at X = −14 R_E at 6:21 UT: (a) coordinate x, (b) velocity v, (c) phase portrait (x,v), and (d) wavelet spectrum of v. Ground BH magnetic field component observed by magnetometers at Rankin Inlet, Nunavut in Canada on 23 March 2009 between 6:00 and 6:40 UT, and their wavelet spectra.

Motion of X-lines: Magnetic reconnection, being a process of rapid energy conversion, plays a key role in magnetospheric dynamics. Some past studies indicate that the reconnection X-line, where the field lines are merged, can move in a specific direction in the magnetotail. A detailed statistical study of X-line motion in the Earth's magnetotail is presented, using in situ multi-spacecraft measurements. The X-line velocity is obtained for 24 reconnection events observed by the *Cluster* spacecraft between 2001 and 2005. The data set consists of 10 single X-lines and 14 X-lines from time intervals of multiple reconnection. Except for two X-lines from multiple reconnection, all the X-lines move tailward (radial outward) along the current sheet, which is consistent with the direction of the pressure gradient. The X-lines also propagate outward from the midnight sector in the dawn-dusk direction. The X-line speed in the Earth-tail direction is comparable and proportional to the reconnection inflow speed, as shown in Fig. 20, and approximately 0.1 of the reconnection outflow speed. These results suggest that both the global pressure distribution and the local reconnection physics may affect the motion of the X-line.

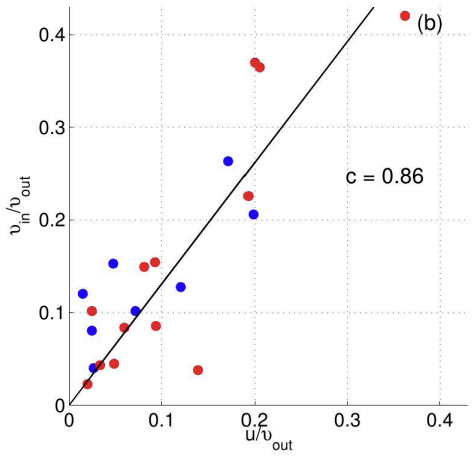

Fig. 20: Reconnection inflow speed versus the X-line speed in radial direction, both normalized to the reconnection outflow speed, c = 0.86 is the correlation coefficient. Black line is the linear regression

Configuration of magnetotail current sheet: Multi-point measurements of magnetic field and plasma parameters by *THEMIS* are used to study the current sheet configuration in the magnetotail. Events are selected when simultaneous crossings of the current sheet took place at three distances downtail, i.e., x<–25 R_E, x~–17 R_E, and x~–10 R_E. The vertical velocity of the current sheet (flapping motion) is determined and based on this velocity, the current sheet thickness L(x) and the current density $j_0(x) \approx (c/4\pi)B_0/L$ are determined. Here $B_0(x)$ is the amplitude of the Earthward component of the magnetic field B_x. Fig. 21 shows two examples of the current sheet parameters.

Multi-event analysis reveals that the current sheet is relatively stable over 1-3 hours. It is also shown that the current sheet can be very stretched, i.e. a large gradient scale of $B_z(x)$, also in the near-Earth region, so that the current sheet has a near one-dimensional configuration. These profiles suggest that the role of the kinetic effects become also important for the current sheet in the near-tail region unlike the expectation that the current sheet configuration is more dipolar like, i.e. a large normal component B_z and/or steeper radial gradient in B_z.

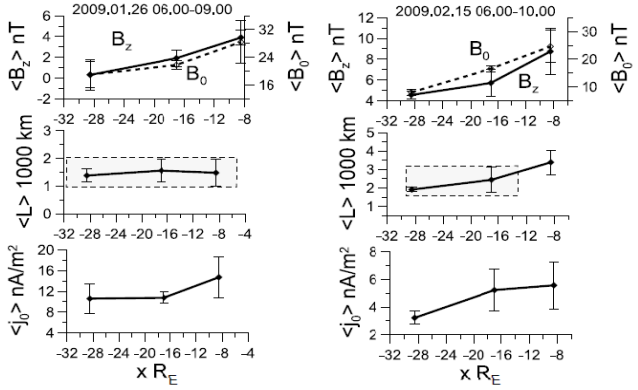

Fig. 21: Current sheet parameters (from top to bottom: normal component of the magnetic field, B_z; current sheet thickness, L; current density, j_0) along the magnetotail shown for four events. Grey boxes show the part of magnetotail current sheet, where almost constant thickness L was observed.

Density derivation using spacecraft potential: *ASPOC* instruments aboard the *Cluster* and *MMS* missions minimize spacecraft charging effects, by reducing the spacecraft potential to values not higher than a few volts. While in operation, *MMS*/*ASPOC* emits indium ion beams with energy ranging between 4-12 keV. Although *ASPOC* operation increases the accuracy of plasma measurements, it prevents from a direct use of the spacecraft potential variation to derive plasma densities. For this reason, a new reconstruction method of uncontrolled spacecraft potential from controlled spacecraft potential data is developed, in order to provide estimates of electron plasma densities in tenuous regions, using multi-spacecraft observations. Data from the *Cluster* mission in the magnetotail region were used for this purpose.

This method was applied for *Cluster* data to obtain photoelectron emission curves between 2001 and 2004. The plasma density profile was then reconstructed using spacecraft potential from data with active spacecraft potential control (Fig. 22). It was found that photoelectron emission and the obtained plasma density exhibit variations over time that were related to solar cycle variations.

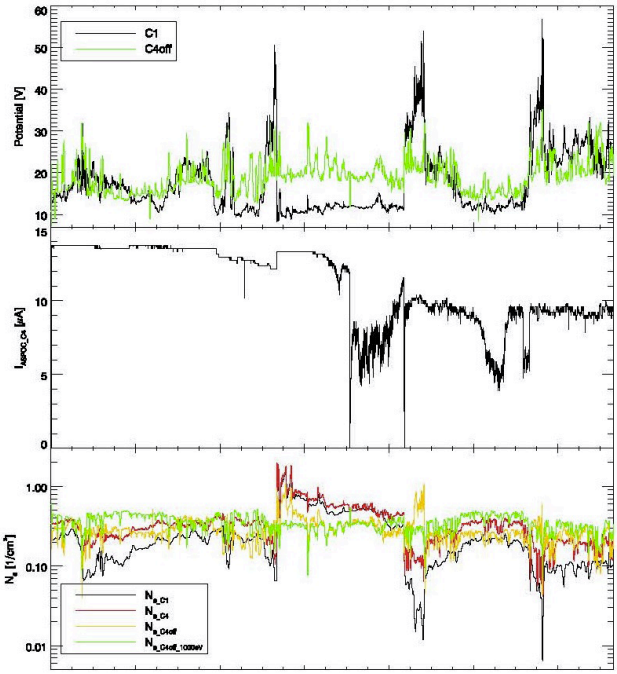

Fig. 22: Spacecraft potential reconstructions and plasma density estimates for a period during August-October 2003, when the spacecraft were orbiting at the tail (a) the reconstructed spacecraft potential (green line) and comparison with the uncontrolled spacecraft potential of another spacecraft (black line), (b) the original spacecraft potential data with *ASPOC* on before the reconstruction, (c) the electron density estimates (green and yellow lines) and comparison with electron density measurement from the *PEACE* particle detector aboard *Cluster*.

SOLAR SYSTEM

IWF is engaged in many missions, experiments and corresponding data analysis addressing solar system phenomena. The physics of the Sun and the solar wind, its interaction with solar system bodies, and various kinds of planetary atmosphere/surface interactions are under investigation.

SUN & SOLAR WIND

The Sun's electromagnetic radiation, magnetic activity, and the solar wind are strong drivers for various processes in the solar system.

SOLAR ORBITER

Solar Orbiter is a future ESA space mission to investigate the Sun, scheduled for launch in 2017. Flying a novel trajectory, with partial Sun-spacecraft corotation, the mission plans to investigate in-situ plasma properties of the near solar heliosphere and to observe the Sun's magnetized atmosphere and polar regions. IWF builds the digital processing unit (DPU) for the *Radio and Plasma Waves (RPW)* instrument aboard *Solar Orbiter* and has calibrated the *RPW* antennas, using numerical analysis and anechoic chamber measurements. Furthermore, the institute contributes to the magnetometer.

Radio and Plasma Waves (RPW): *RPW* will measure the magnetic and electric fields at high time resolution and will determine the characteristics of the magnetic and electrostatic waves in the solar wind from almost DC to 20 MHz. Besides the 5 m long antennas and the AC magnetic field sensors, the instrument consists of four analyzers: the thermal noise and high frequency receiver; the time domain sampler; the low frequency receiver; and the bias unit for the antennas. The control of all analyzers and the communication will be performed by the DPU, developed by IWF.

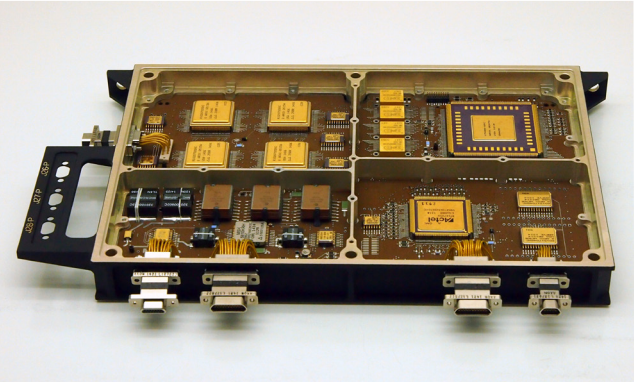

Fig. 23: Flight model of the DPU or the *RPW* instrument aboard *Solar Orbiter*.

The DPU EM4 qualification model and, at the end of 2015, the first flight model of the DPU (Fig. 23) have been delivered to LESIA, Observatoire de Paris. Large effort has been made for a solder qualification for three packages used in the DPU. One is the 3DPlus EEPROM, which consists of a stack of eight memory components. Because of its unusual height, this package is very sensitive to vibration loads and the solder process is critical. A test board with 3DPlus components and LCC3 packages has been built, vibration tested and thermally stressed over 200 cycles (full temperature range). Finally, the solder joints have been inspected by micro-sectioning. The results are positive and IWF is certified to solder these components. For the third component the micro-sectioning is still ongoing. Furthermore, a detailed analysis and qualification program has been executed for the FPGA design. In cooperation with French specialists the design has been reviewed, simulated, tested and an extensive statistics has been established, demonstrating the compliance with the ESA ESCC design rules.

PHYSICS

The kinetic slow mode as a candidate process for solar wind heating: The solar wind exhibits various kinds of broadband fluctuations in the magnetic field, ranging from mHz to tens of Hz in frequency. Solar wind turbulence at frequencies around 1 Hz is particularly interesting and important in understanding the dissipation mechanism of magnetohydrodynamic turbulence by ion motion and the heating mechanism in the solar wind. Yet what kind of fluctuation modes rule the heating mechanism through wave-particle interactions? A theoretical plasma wave study has revealed the possible existence of the kinetic slow mode in the solar wind on spatial scales around the ion gyro-radius (~100-1000 km in the solar wind). The kinetic slow mode represents the lowest-frequency compressible waves propagating quasi-perpendicular to the mean magnetic field on the ion gyro-radius scales (Fig. 24) and can heat the solar wind ions through proton Landau resonance. The properties of the kinetic slow mode are studied, and the mode is testable against the solar wind observations.

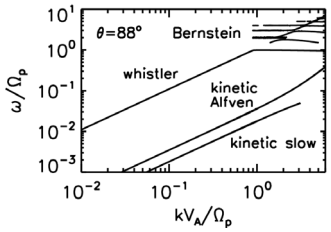

Fig. 24: Dispersion relations for kinetic slow, kinetic Alfvén, whistler, and ion Bernstein modes are theoretically evaluated in the diagram spanning the wave numbers normalized to the proton inertial length on the x-axis and the frequencies normalized to the proton gyro-frequency on the y-axis.

A new process for strong non-radial eruptions of solar coronal mass ejections: On 7 January 2014, one of the fastest CMEs of the current solar cycle, with an initial speed of about 2500 km/s, erupted from solar disk center. Major alerts were sent out by space weather prediction offices such as NOAA because the CME was thought to be Earth directed, which lead to a global news coverage of the event. However, it turned out very unexpectedly that the CME missed Earth almost entirely, and no significant geomagnetic activity followed. To figure out the causes, data provided by the Heliophysics System Observatory were analyzed, from *STEREO-A* and *B, SOHO, SDO, Wind, Mars Express*, and the radiation instrument on the *Curiosity* rover on Mars.

For connecting the observations from the Sun to the planets, the Ellipse Evolution (ElEvo) model was introduced for the CME shock based on hydrodynamic drag equations and an elliptic shape. The model can analytically predict planetary CME shock arrival times and speeds and can also be used in real time. From *STEREO, SDO* and *SOHO* imaging it could be unambiguously derived that a CME erupted from the source region to about 40° west of Earth, confirmed by a Forbush decrease at Mars and the arrival of a weak shock at Wind (Fig. 25). This is the strongest non-radial eruption of a CME that has ever been observed. The cause for the eruption was a "channeling" by the active region magnetic fields, which is a so far largely unrecognized process. It has been further confirmed with other studies on modeling the coronal magnetic fields of the active region producing this CME.

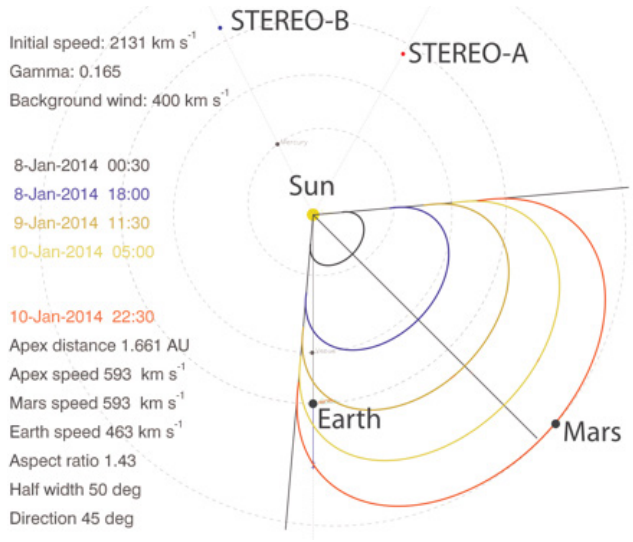

Fig. 25: Heliospheric positions of various planets and spacecraft on 7 January 2014. The shape of the CME shock given by ElEvo is plotted for different time steps as indicated by colors.

Statistical description of magnetic fluctuations in the solar wind: The interplanetary magnetic field exhibits fluctuations over a huge range of temporal and spatial scales. Although the variability of fluctuations is high and the number of involved physical processes is large, statistical physics offers a reduction scheme, in which the scale dependent histograms can be explained in terms of a limited set of theoretical probability distribution functions. Unconditional and conditional statistics based on thresholding of physical parameters has revealed, that the histograms of magnetic fluctuations associated with multi-scale or inertial-range turbulent processes during alternating high-speed low-speed solar wind streams, can be described in terms of additive and multiplicative processes with or without correlations. It was shown that the additive normal (P_n) and multiplicative log-normal (P_{Ln}) theoretical distributions represent a limiting case of kappa (P_κ) and log-kappa ($P_{L\kappa}$) distributions. In terms of correlations, the transition from long-range (log-)kappa to short-range (log-)normal correlations is obtained in the limit of $\kappa \rightarrow \infty$, where κ is the so-called non-extensivity parameter. The results suggest that the kappa family of model distribution functions offers the desirable flexibility in statistical modeling of interplanetary magnetic field fluctuations (Fig. 26).

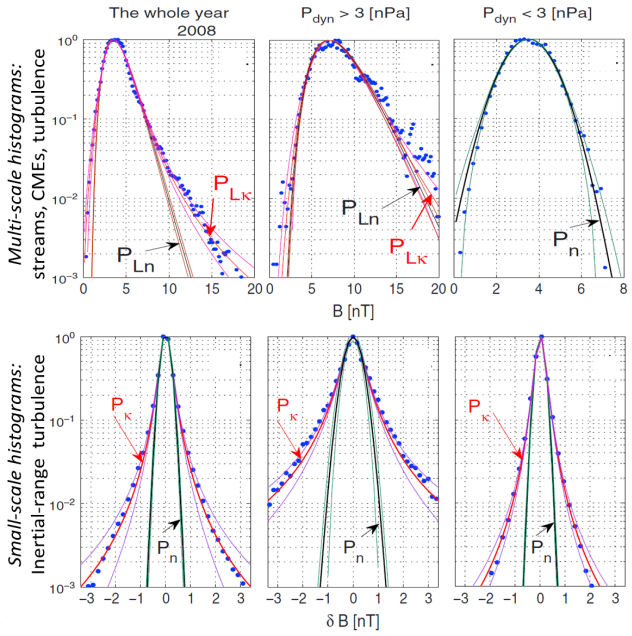

Fig. 26: Probability distribution functions from the direct measurements in the solar wind. Top: multi-scale histograms; bottom: inertial range histograms; left: unconditional statistics; center/right: conditional statistics based on thresholding. Theoretical distributions: P_n - normal, P_{Ln} - log-normal P_κ - kappa, $P_{L\kappa}$ - log-kappa distribution functions.

MERCURY

Mercury is now in the center of attention because of the current NASA *MESSENGER* mission and the upcoming ESA/JAXA *BepiColombo* mission. The planet has a weak intrinsic magnetic field and a mini-magnetosphere, which strongly interacts with the solar wind.

BEPICOLOMBO

Two spacecraft, to be launched in 2018, will simultaneously explore Mercury and its environment: the Japanese *Magnetospheric (MMO)* and ESA's *Planetary Orbiter (MPO)*. IWF plays a major role in developing the magnetometers for this mission: it is leading the magnetometer investigation aboard the *MMO (MERMAG-M)* and is responsible for the overall technical management of the *MPO* magnetometer *(MERMAG-P)*. For *MPO*, IWF also leads the development of *PICAM*, an ion mass spectrometer with imaging capability, which is part of the *SERENA* instrument suite, to explore the composition, structure, and dynamics of the exo-ionosphere.

During 2015, the instrument teams at IWF supported system level testing of both *MMO* and *MPO* spacecraft (Fig. 27). It included e.g. detailed functional and electromagnetic compatibility tests. The IWF magnetometer group assembled the *MERMAG-P* spare model and finished all related environmental tests.

For *PICAM* the main task in 2015 was the completion of the flight model campaign and the refurbishment of the qualification model as flight spare. The flight model was delivered to ESA by the end of March, and it was integrated on *MPO* in exchange with the qualification model. The latter was upgraded to be flight capable by the end of 2015.

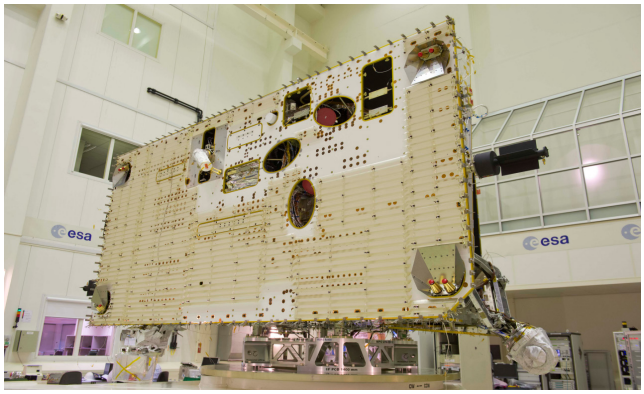

Fig. 27: The proto-flight model of the *BepiColombo Mercury Planetary Orbiter (MPO)* in the test center at ESA's European Space Research and Technology Centre (Credits: ESA/A. Le Floc'h).

PHYSICS

Long-term rotational state and spin-orbit coupling of Mercury: Together with the Departments of Mathematics of the Universities of Namur (Belgium) and Milan (Italy), the long-term behavior of the coupling between the rotational state and the orbital motion of Mercury (which is currently in a 3:2 spin-orbit resonance) has been investigated. The study allows providing bounds (in the order of 0.1 rad) to both the latitudinal and longitudinal libration angles for a long but finite time. The main conclusion is that Mercury's current spin-orbit coupling is practically stable (and may persist for orders of magnitude exceeding the age of the solar system).

Mercury's surface-exosphere environment: The efficiency of sputtered elements by H^+ and He^{2+} solar wind ions from Mercury's surface and their contribution to the exosphere have been studied for various solar wind conditions. A 3D solar wind–planetary interaction hybrid model was used for the production of particle precipitation maps on the surface. The sputter yields are calculated by coupling a surface-plasma interaction model with a 3D exosphere model. Due to Mercury's magnetic field, for moderate solar conditions the plasma precipitates only around the poles. For extreme solar events (i.e., fast solar wind, CMEs), the solar wind plasma has access to the entire dayside area. In such cases the release of particles from the planet's surface can result in an exospheric density increase of more than one order of magnitude. The escape rates are also about an order of magnitude higher. Furthermore, the amount of He^{2+} ions in the precipitating solar plasma flow enhances also the release of sputtered elements from the surface in the exosphere. The modelled results are in good agreement with *MESSENGER* satellite observations of sputtered Mg and Ca elements, shown in Fig. 28.

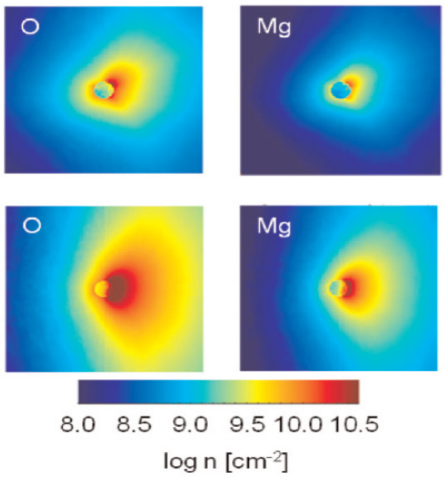

Fig. 28: Column densities for a moderate a slow and fast solar wind case of sputtered O and Mg along the Sun-planet direction at 10 Mercury radii and projecting the density integrated along the lines of sight onto the noon-midnight plane.

VENUS & MARS

Two terrestrial planets are located just inside, Venus at 0.7 AU (AU = Astronomical Unit, distance Earth-Sun), and just outside, Mars at 1.5 AU, of the Earth's orbit around the Sun. Venus has a radius slightly smaller than Earth and is differentiated; it does, however, not exhibit an internal magnetic field. Mars has a radius about half as big as that of the Earth, is also differentiated, but only exhibits remnant surface magnetization of a now defunct internal dynamo. Venus is characterized by a very dense atmosphere, whereas Mars has a very tenuous one. Both planets generate a so-called induced magnetosphere by their interaction with the solar wind.

INSIGHT

The planned March 2016 launch of NASA's *InSight* mission to Mars had to be suspended due to problems with the prime instrument. IWF is contributing to the *HP*^{3} (mole) experiment, which is to explore the mechanical properties of the Martian soil as the mole penetrates the ground to a planned depth of about 3 m.

A so-called "pile driving model" was developed, which is able to predict the displacement of the mole in the soil in response to subsequent hammer strokes. Fig. 29 shows the displacement of the mole elements caused by a single hammer stroke in a cohesionless material.

For a more accurate simulation of the soil response, a particle-code called LIGGGHTS was used. Thereby it is possible to calculate the soil deformation and the local changes of density due to the mole penetration. A coupling of a multi body system of the hammer mechanism and the soil model allows also for efficiency investigations at different depths.

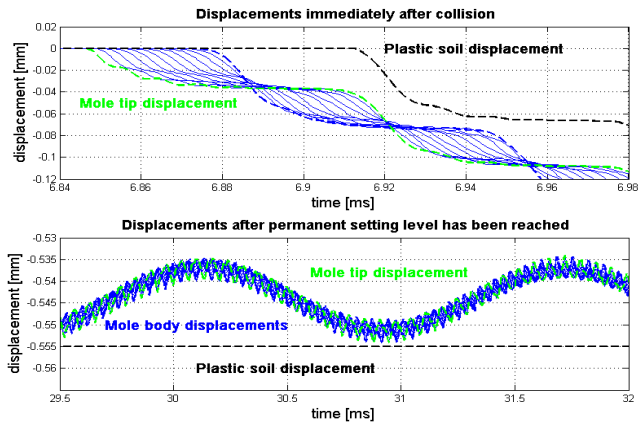

Fig. 29: Displacement of the mole elements and plastic displacement of the soil around the tip immediately after a hammer stroke, as calculated by the "pile driving model" for mole penetration.

CHINESE MARS MISSION

China plans a Mars orbiter and lander to be launched in 2022. The main mission will conduct a comprehensive remote sensing and a surface landing on the Red Planet. IWF will contribute a magnetometer.

PHYSICS

Venusian ionosphere: Examination of *Venus Express (VEX)* low altitude ionospheric magnetic field measurements during solar minimum has revealed the presence of strong magnetic fields at low altitudes over the north pole of Venus. 77 events with strong magnetic fields as *VEX* crossed the northern polar region were identified between July 2008 and October 2009 (Fig. 30). These events all have strong horizontal fields, slowly varying with position. They do not show a preference for any particular Interplanetary Magnetic Field (IMF) orientation. However, they are found over the geographic pole more often when the interplanetary field is in the Venus orbital plane than when it is perpendicular to it. The structures were found most frequently in the -E hemisphere, determined from the IMF orientation. The enhanced magnetic field is mainly quasi perpendicular to solar wind flow direction and it is suggested that these structures form in the low altitude collisional ionosphere where the diffusion and convection times are long.

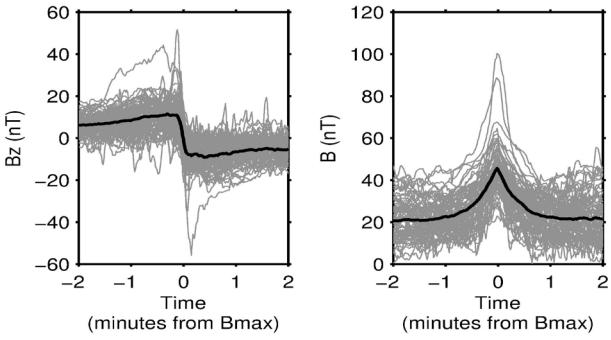

Fig. 30: Superimposed magnetic field profiles of the 77 selected events. Note that the magnetic field Bz component of the structures have been transformed into the same bipolar directions.

Venus proton cyclotron waves (PCW) near solar maximum: Already in the first years of *VEX* in solar minimum the magnetometer data allowed to identify PCWs in the regions upstream of the Venus bowshock. These waves are a tracer for newborn planetary H^+ ions, escaping from the planet's exosphere and being lost to the solar wind. The escape of H from Venus and Mars has an important influence on the different evolution of their respective atmosphere over the timespan of the solar system evolution. Now the magnetometer data were investigated for the occurrence of upstream PCWs for two Venus years, when the solar activity was near its maximum. Surprisingly, more wave occurrences were found, although

the solar wind is expected to be more turbulent and less favorable for such wave generation for maximum conditions. Also, the waves were mainly found for times with IMF pointing towards the Sun, but their overall properties were similar to those at solar minimum. An explanation for the unexpected results was found from the specific solar wind conditions for the unusual solar maximum. The solar maximum was very weak, with times of extremely low proton density and low to medium velocity. Still the higher UV emission leads to an increase in the generation of newborn Venusian protons against a background of very low solar wind density. The thus enhanced ratio of plan-etary protons to solar wind protons is the driver for the increased generation of PCWs. Furthermore, it was found that the asymmetry in the wave occurrence is due to the southward tilt of the solar current sheet with prevailing inward IMF polarity in the northern lobe for this solar maximum. Since the *VEX* orbit is approximately in the ecliptic plane, it is mainly above the tilted current sheet in the northern lobe and the magnetometer will observe more inward polarity for the specific time interval investigated.

JUPITER & SATURN

Jupiter and Saturn are the two largest planets in the solar system. Because of their atmospheric composition they are called "gas giants". Both planets rotate rapidly (approximately with a 10 hours period) and are strongly magnetized, with the Jovian multipole field tilted at 10° and the Kronian field almost dipolar and perfectly aligned with the rotational axis. The magnetospheres are dominated by internal plasma sources, generated by the large number of moons, particularly Io at Jupiter and Enceladus at Saturn. The gas giants are also strong sources of radio emissions.

CASSINI

The *Cassini* mission is in its 11th year since Saturn orbit insertion. In 2015 *Cassini* performed the last equatorial orbits and the last flybys of the moons Dione and Enceladus during its long mission. In 2016 flybys at Saturn's largest moon Titan will be used to raise its orbital inclination over 60°. IWF participated in *Cassini* with the *Radio and Plasma Wave Science (RPWS)* instrument.

JUICE

ESA's first Large-class mission *JUpiter ICy moons Explorer (JUICE)* is planned for launch in 2022 and arrival at Jupiter in 2030. In 2015, the contract for building the *JUICE* spacecraft was signed by ESA and Airbus Defence and Space (Fig. 31). *JUICE* will spend at least three years making detailed observations of the giant gaseous planet Jupiter and three of its largest moons, Ganymede, Callisto and Europa. IWF is taking part with Co-I-ship for three different selected instrument packages.

For the *Jupiter MAGnetometer (J-MAG)* IWF supplies an atomic scalar sensor, which is developed in collaboration with TU Graz. In 2015, the design of *J-MAG* was consolidated and the manufacturing of the laboratory model has been started. The *Particle Environment Package (PEP)* is a plasma package with sensors to characterize the plasma environment in the Jovian system and the composition of the exospheres of Callisto, Ganymede, and Europa. IWF participates in the *PEP* consortium on Co-I basis in the scientific studies related to the plasma interaction and exosphere formation of the Jovian satellites. IWF is also responsible for the antenna calibration of the *Radio and Plasma Wave Investigation (RPWI)* instrument. Numerical simulations for a configuration of three dipoles mounted on the magnetometer boom have shown that the exact positions of the feed points are crucial for the antenna reception properties.

Fig. 31: Artist's impression of the *JUICE* spacecraft in the Jupiter system (Credits: Airbus Defence and Space).

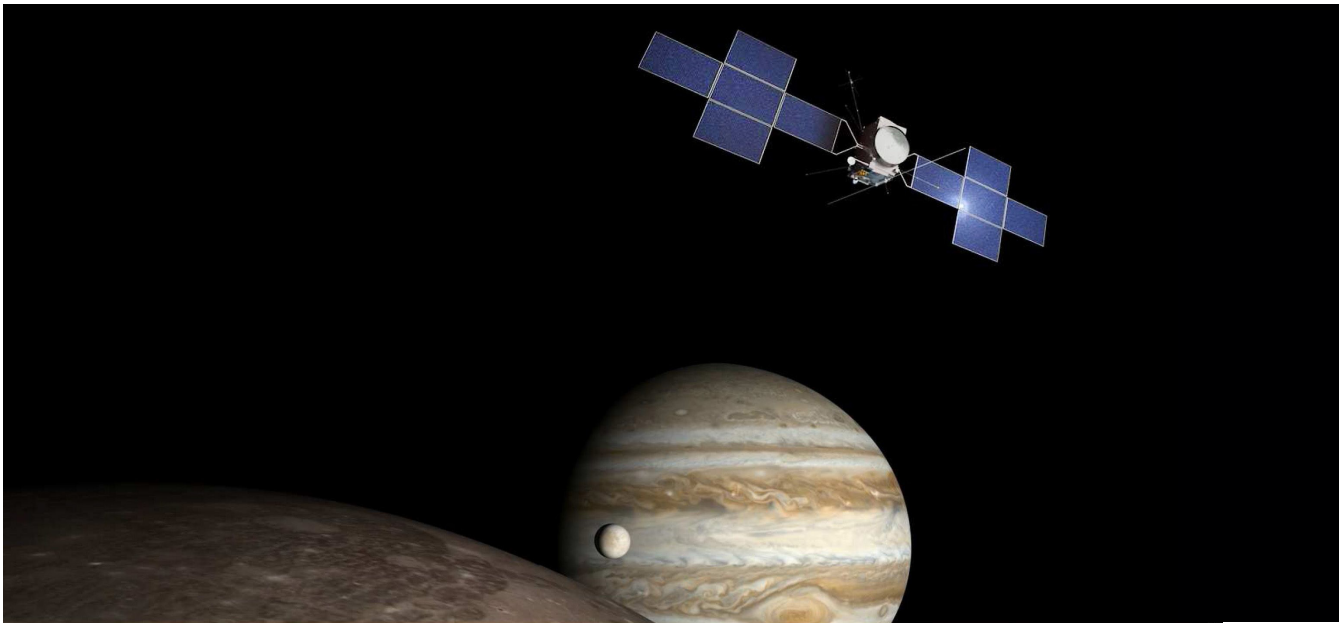

COMETS & DUST

Comets and interplanetary dust are the remainders of the building blocks from which the solar system was formed, although dust can also be created by collisions of e.g. asteroids. With the arrival of *Rosetta* at comet 67P/Churyumov-Gerasimenko the study of comets has started again after a few decades since the last cometary mission.

ROSETTA

Rosetta arrived at comet 67P/Churyumov-Gerasimenko (67P/CG) in August 2014 and has since followed the comet along its orbit past perihelion (Fig. 33). The nominal mission ended at the end of 2015, however, it has been extended until September 2016.

IWF is participating in five instruments, on PI basis for the *Micro-Imaging Dust Analysis System (MIDAS)* and Co-I basis for the *Rosetta Plasma Consortium (RPC)*, the *Rosetta Lander Magnetometer and Plasma Monitor (ROMAP)*, the *Multi-Purpose Sensor (MUPUS)*, and the *Cometary Secondary Ion Mass Spectrometer (COSIMA)*.

PHYSICS

Location and stability of µm-sized dust particles in the solar system: Together with the Department of Mathematics of the University of Rome Tor Vergata (Italy), the possibility of stable motions of µm-sized dust particles in the vicinity of the Lagrange points L4, L5 in the solar system (as well as in planetary systems) has been investigated. Conditions on the physical parameters (size, density, optical properties), which are necessary for temporary capture, have been derived.

It turned out that the time of temporary capture (stability time) close to the tadpole regime of motion is strongly affected by solar radiation, i.e. by the so-called Poynting-Robertson effect caused by relativistic particle–photon interactions. For 10-100 µm sized particles, the orbital stability is only 1000-10000 years.

Gravity field and rotational state of comet 67P/C-G: In collaboration with the department SYRTE (Systèmes de Référence Temps-Espace) of the Observatoire de Paris IWF successfully determined the gravity field and the basic rotational properties (Fig. 34) of comet 67P/C-G. The results are based on a polyhedron model of the comet's nucleus, obtained from the *OSIRIS* and *NAVCAM* experiments aboard the *Rosetta* spacecraft.

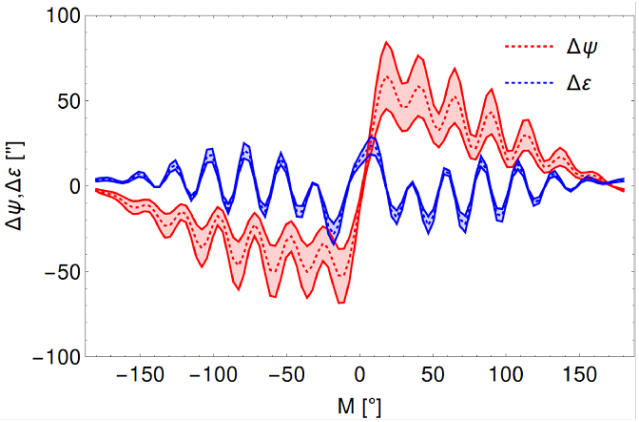

Fig. 34: Nutation parameters (caused by solar torque) versus mean anomaly M for normalized polar moment of inertia c=0.25. Dotted lines: actual parameters; shaded regions: possible offsets due to outgassing effect.

Fig. 33: Images of comet 67P/C-G taken with *OSIRIS* narrow-angle camera on 12 August 2015, just a few hours before the comet reached perihelion, about 330 km from the comet (Credits: ESA/Rosetta/MPS for OSIRIS Team MPS/UPD/LAM/IAA/SSO/INTA/UPM/DASP/IDA).

EXOPLANETARY SYSTEMS

The field of exoplanet research (i.e. investigation of planets around stars other than our Sun) has developed strongly, in the past decade. Since the discovery of 51 Peg b, the first Jupiter-type gas giant outside our Solar System, more than 1000 exoplanets, about 800 planetary systems with more than 170 multiple planet systems have been detected. Better observational methods have led to the finding of so-called super-Earths, some of them even inside the habitable zone of their host star. However, the majority of super-Earths have low average densities, which indicate that they are surrounded by dense hydrogen envelopes or volatiles. By minimizing the uncertainties of the radii with the upcoming missions *CHEOPS* and *PLATO*, densities and hence the structure of these planets will be better determined.

The institute concentrates on the study of planetary atmospheres using both theory and observation, focusing on the analysis of exoplanet evaporation and mass loss processes. Further research is conducted towards star-planet interaction phenomena through the collection and analysis of transmission and emission exoplanet observations.

CHEOPS

ESA's first Small-class mission *CHEOPS (CHaracterizing ExOPlanets Satellite)* will be the first space mission dedicated to characterize exoplanets in detail. It will focus on exoplanets with typical sizes ranging from Neptune down to Earth diameters orbiting bright stars. This mission will also try to specify the components of their atmospheres.

The electrical subsystem for *CHEOPS* consists of two units, the *BEE (Back-End-Electronics)* and the camera. IWF is responsible for the development of the fully redundant *BEE*. The institute develops the DPU (digital processing unit) and its boot software, while the PSU (power supply unit) is a contribution of RUAG Space Austria. The *BEE* provides the electrical interface to the spacecraft and performs the control of the *CHEOPS* instrument. Commands are routed from the spacecraft through the *BEE* to the camera and the image data are compressed and packetized for transmission.

The preliminary design review for the *BEE* has been successfully completed and the development of the DPU prototypes was started. In parallel, the *BEE* Structural and Thermal Model (STM) was assembled by IWF and delivered to Airbus Spain (Fig. 35). The vibration tests at spacecraft level have been successfully finished. The first prototype was integrated with the power supply into an electrical representative *BEE* model. The delivery to Airbus is scheduled for the first quarter of 2016. Two more DPU prototypes have been assembled and tested. One has been delivered to the Institute of Astronomy of the University of Vienna for the development of the application software, while the last one remains at the institute as reference for the boot S/W development. Presently, the Engineering and Qualification Model (EQM) of the DPU is built. The integration of the BEE EQM is scheduled for the beginning of 2016.

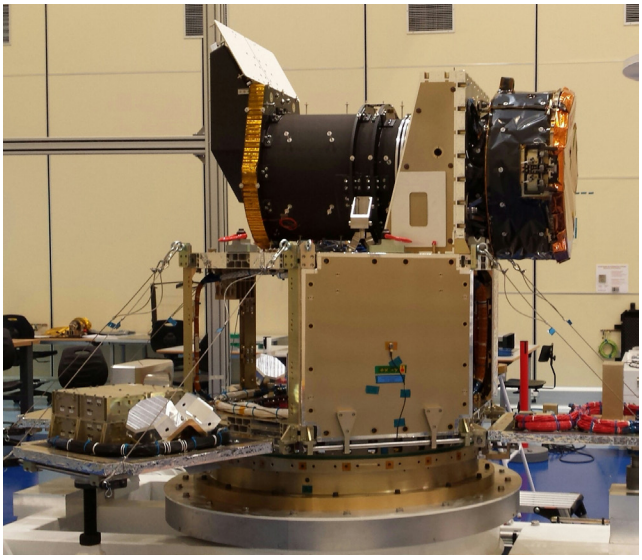

Fig. 35: Structural model of the *CHEOPS* spacecraft during preparation for vibration test. The *BEE* STM, can be seen on the folded-out panel at the left side.

PLATO

PLATO (PLAnetary Transits and Oscillations of stars, Fig. 36) is the third Medium-class mission in ESA's Cosmic Vision program. It will monitor relatively nearby stars, searching for tiny, regular dips in brightness as their planets transit, temporarily blocking out a small fraction of the starlight. By using 34 separate small telescopes and cameras, *PLATO* will search for planets around up to a million stars spread over half of the sky. It will also investigate seismic activity in the stars, enabling a precise characterization of the host star of each planet discovered, including its mass, radius and age. *PLATO* will identify and study thousands of exoplanetary systems, with an emphasis on discovering and characterizing Earth-sized planets and super-Earths in the habitable zone of their parent star – the distance from the star where liquid surface water could exist.

IWF together with the Institute of Astrophysics (IfA), University of Vienna, is participating in the development of the on-board *PLATO* data processing chain. The *PLATO*

instrument will search for planets around up to a million stars, measuring the small variations in brightness by high precision photometry. Sixteen digital processing units and two so called "fast DPUs" will process the image data. The pre-processed information will be routed to the instrument control unit (ICU), where it needs to be compressed and packetized for the telemetry transfer. The front end of the ICU builds the *Router and Data Compression Unit (RDCU)*, built by IWF and IfA, which combines two functions. On one hand it bundles the SpaceWire channels from the six DPUs and six ancillary units into one link to the memory in the instrument controller. In addition, it provides a fast data compressor realized by hardware logic in an FPGA.

PHYSICS

On the stellar activity – planet surface gravity correlation of systems hosting hot Jupiters: The chromospheric ativity index $\log R'_{HK}$ of stars hosting transiting hot Jupiters appears to be correlated with the planets' surface gravity. One of the possible explanations is based on the presence of condensations of planetary evaporated material located in a circumstellar cloud that absorbs the CaII H&K and MgII h&k resonance line emission flux, used to measure chromospheric activity. A larger column density in the condensations, or equivalently a stronger absorption in the chromospheric lines, is obtained when the evaporation rate of the planet is larger, which occurs for a lower gravity of the planet. This selection based on the systems' interstellar reddening was considered to minimize systematic effects on the $\log R'_{HK}$ measurements. A mixture model was applied to the data ($\log R'_{HK}$ values and planets' surface gravities) gathered for the selected sample of systems. It was found that the data are best fit by a two-linear-regression model. This result was interpreted in terms of the Vaughan-Preston gap. A Monte Carlo approach led to conclude that the two intercepts fit the observed peaks of the distribution of $\log R'_{HK}$ for main-sequence solar-like stars (see Fig. 36).

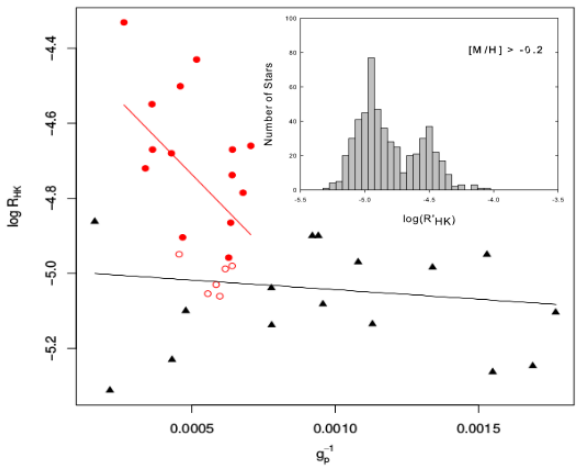

Fig. 36: Chromospheric emission index $\log R'_{HK}$ vs. inverse of the planet surface gravity for the considered systems with the two best-fitting regression lines of the mixture model in black and red. The open circles show systems that could belong to either correlation.

The intercepts also correlate with the slopes, as predicted by the model based on the condensations of planetary evaporated material. These findings bring further support to the model, although it was not possible to firmly exclude different explanations, such as star-planet interactions.

Deep mixing effects in starspot variability: The current knowledge on plasma convective mixing in stellar interiors is based on theoretical modelling, which provides the basis for the empirical relations between the mixing and observable stellar parameters. A model-independent approach to study the mixing process is still a challenge. The new spectral-correlation method, verified for the Sun and applied to the Kepler mission photometry of main sequence stars, shows that deep mixing is manifested in stellar photometric light curves. The timescales of the stochastic change in the spectral power of stellar rotational variability were measured for first and second rotational harmonics of hundreds of Kepler stars. These timescales, which characterize the dynamics of global starspot patterns have been shown to obey Kolmogorov's theory of turbulence.

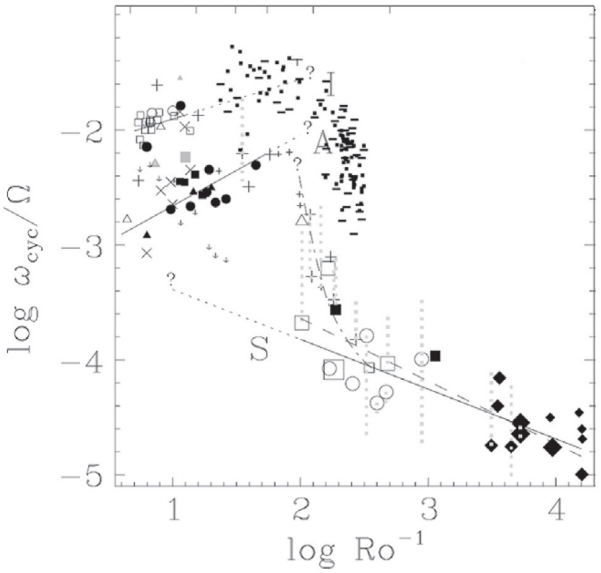

Fig. 37: The relation between normalized cyclic frequency ωcyc of stellar activity cycles and the inverted Rossby number Ro^{-1}.

Deep mixing affects the relation between the cyclic frequency ω_{cyc} of short-periodic activity cycles and the inverted Rossby number $Ro^{-1} \propto \tau$ (Fig. 38), where τ is the characteristic timescale of deep mixing, known as the turnover time in the standard mixing length theory. It has been shown that τ can be found by the conversion of the measured timescales of the first and second rotational harmonics into the timescale of laminar convection. This connection opens the way to determine the model-independent turn-over time. The discovered new branch on the ω_{cyc} - Ro^{-1} diagram (the central cluster in Fig. 37) connects the branch of inactive stars with the area populated by super-active objects. The formation of the discovered branch is due to the α-quenching effect, which saturates the magnetic dynamo and decreases the cycle periods with the increase of Ro^{-1}.

INFRASTRUCTURE

Instruments aboard spacecraft are exposed to harsh environments, e.g., vacuum, large temperature ranges, radiation, and high mechanical loads during launch. Furthermore, these instruments are expected to be highly reliable, providing full functionality over the entire mission time, which could last for more than a decade.

VACUUM CHAMBERS

The *Small Vacuum Chamber* is a manually controlled, cylindrical vacuum chamber (160 mm diameter, 300 mm length) for small electronic components or printed circuit boards. It features a turbo molecular pump and a rotary dry scroll forepump. A pressure level of 10^{-10} mbar can be achieved.

The *Medium Vacuum Chamber* has a cylindrical stainless steel body with the overall length of 850 mm and a diameter of 700 mm. A dry scroll forepump and a turbo molecular pump provide a pressure level of about 10^{-7} mbar. A target manipulator with two axes and an ion beam source are installed. This chamber mainly serves for functional tests of the ion mass spectrometer for *BepiColombo*.

The *Large Vacuum Chamber* has a horizontal cylindrical stainless steel body and door, a vision panel, two turbo molecular pumps and a dry scroll forepump. A pressure of 10^{-7} mbar can be achieved. The cylinder has a diameter of 650 mm and a length of 1650 mm. During shutdown the chamber is vented with nitrogen. A target manipulator inside the chamber allows for computer-controlled rotation of the target around three mutually independent perpendicular axes. The vacuum chamber is enclosed by a permalloy layer for magnetic shielding. To enable the baking of structures and components (to outgas volatile products and unwanted contaminations), the chamber is equipped with a heater around the circumference.

The *Thermal Vacuum Chamber* is fitted with two turbo molecular pumps, a dry scroll forepump, and an ion getter pump, which together achieve a pressure level of 10^{-6} mbar and allow quick change of components or devices to be tested. A thermal plate installed in the chamber and liquid nitrogen are used for thermal cycling in a temperature range between -90 °C and +140 °C. The vertically oriented cylindrical chamber allows a maximum experiment diameter of 410 mm and a maximum height of 320 mm.

The *Surface Laboratory Chamber* is dedicated to surface science research. It has a diameter of 400 mm and a height of 400 mm, extendable up to 1200 mm. One rotary vane pump and one turbo-molecular pump achieve a minimum pressure of 10^{-5} mbar. With an external thermostat the chamber temperature can optionally be controlled between -90 °C and +50 °C.

The *Sample Chamber* contains an 8µ particle filter and allows measurements of grain sample electrical permittivity. One rotary vane pump achieves a minimum pressure of 10^{-3} mbar.

HIGH-PERFORMANCE COMPUTER LEO

The new high-performance computer LEO comprises a login-server for job processing and 32 compute nodes with a total of 1320 CPU cores. The software library is implemented with so-called "environment modules", which enable users to quickly include one specific software version, while other users might need a different version. For large-scale simulations there is an attached storage server that provides some 150 TB of hard disk space with different backup levels. The compute nodes use solid-state drives (SSD) for a massive-parallel cluster filesystem. Crucial for high-performance computing is also the 40 Gbit/s network with nanoseconds latency, which is implemented fully by Infiniband hardware. Emergency procedures documentation allows for a complete re-installation of the operating system within about two hours working time. The LEO hardware, shown in Fig. 38, automatically downloads and processes data from the *MMS* mission and is actively used for simulation-based research.

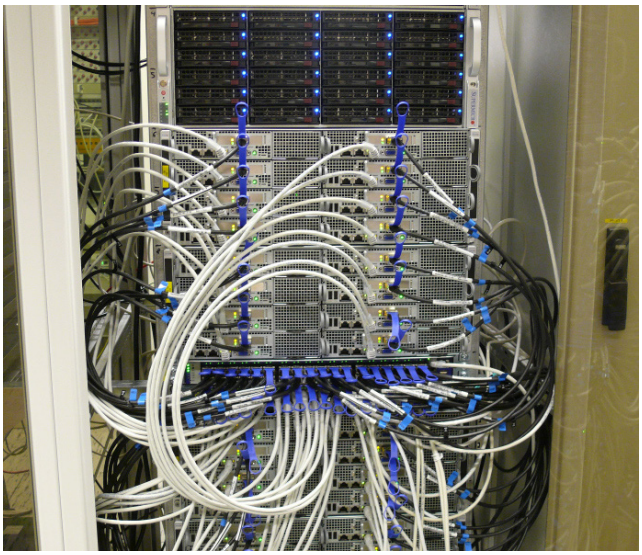

Fig. 38: LEO storage server and compute nodes.

OTHER TEST FACILITIES

The *Temperature Test Chamber* allows verifying the resistance of electronic components and circuits to most temperatures that occur under natural conditions, i.e., -40 °C to +180 °C. The chamber has a test space of 190 l and is equipped with a 32-bit control and communication system.

The second *Temperature Test Chamber* is used for fast cycling electronic components and circuit. The temperature range is -70 °C to +180 °C. The chamber has a test space of 37 l and is equipped with similar interfaces for communication.

The *Penetrometry Test Stand* is designed to measure mechanical soil properties, like bearing strength. The UV Exposure Facility is capable to produce radiation between 200-400 nm (UV-A, UV-B, UV-C).

Magnetometer calibration: A three-layer magnetic shielding made from mu-metal is used for all basic magnetometer performance and calibration tests. The remaining DC field in the shielded volume is <10 nT and the remaining field noise is <2 pT/√Hz at 1 Hz. A special Helmholtz coil system allows generating field vectors of up to ±30000 nT around the sensor under test.

The *Magnetometer Temperature Test Facility* is used to test magnetic field sensors between -170 °C and +220 °C in a low field and low noise environment. Liquid nitrogen is the base substance for the regulation, which is accurate to ±0.1 °C. A magnetic field of up to ±100000 nT can be applied to the sensor during the test cycles.

FLIGHT HARDWARE PRODUCTION

Clean room: Class 10000 (according to U.S. Federal Standard 209e) certified laboratory with a total area of 30 m^2. The laboratory is used for flight hardware assembling and testing and accommodates up to six engineers.

Clean bench: The laminar flow clean bench has its own filtered air supply. It provides product protection by ensuring that the work piece in the bench is exposed only to HEPA-filtered air (HEPA = High Efficiency Particulate Air). The internal dimensions are 118 x 60 x 56 cm^3.

Vapor phase and IR soldering machine: The vapor phase soldering machine is suitable for mid size volume production. The maximum board size is 340 x 300 x 80 mm^3. Vapor phase soldering is currently the most flexible, simplest and most reliable method of soldering. It is ideally suited for all types of surface mounted device (SMD) components and base materials. It allows processing of all components without the need of any complicated calculations or having to maintain temperature profiles. For placing of fine pitch parts and rework of electronic boards an infrared soldering and precision placing system is used.

The new DispenseMate 585 (Fig. 39) is a solder paste printer in a compact benchtop format. This machine allows a precise dosing of solder pastes on PCBs. As an option, a dispenser for precise glue application can be used. The range of motion is 525 x 525 mm.

Fig. 39: Solder paste printer.

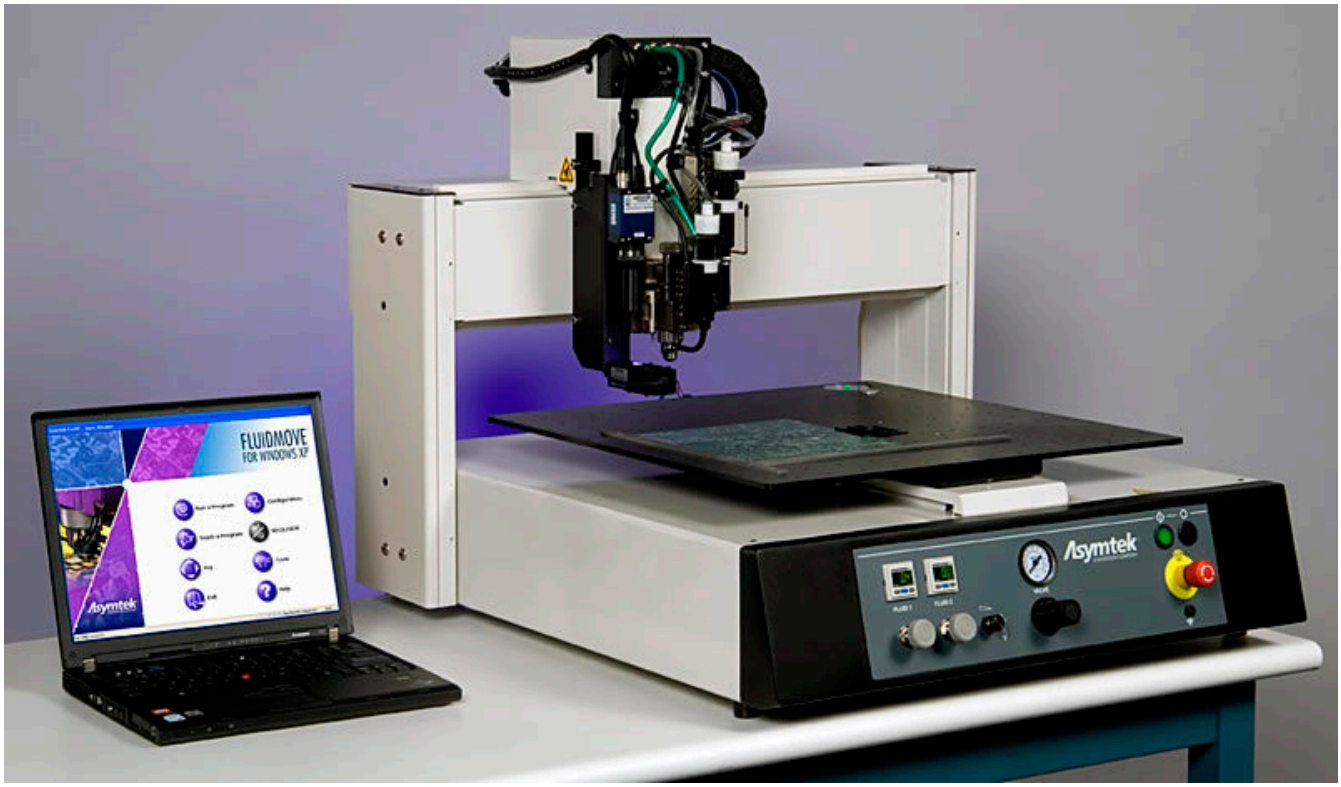

OUTREACH

PUBLIC OUTREACH

IWF is actively engaged in science education and public outreach. 2015 PR activities again concentrated on ESA's comet chaser Rosetta.

From 29 April to 4 May, the "Space Technology 2015" symposium took place during the Graz Spring Fair. IWF participated in the exhibition "Faszination Raumfahrt" and presented numerous payload models of the *BepiColombo*, *COROT*, *Venus Express*, *MMS*, and *Rosetta* missions to over 40000 visitors. On 30 April, special guest Matt Taylor (Fig. 40), ESA *Rosetta* Project Scientist, talked about how to land on a comet and IWF director Wolfgang Baumjohann presented IWF's contributions to this mission.

Fig. 40: ESA Rosetta Project Scientist Matt Taylor and fans during the Graz "Space Technology 2015" symposium.

During the URANIA symposium *"Rosetta & Philae"*on 29 May several IWF members reported about the first results of this outstanding ESA mission.

On 2 October, Deputy Mayor Martina Schröck organized the second "Grazer Weltraumtag" in downtown Graz, which was visited by about 2000 people. IWF guided the visitors to the distant worlds of comets and exoplanets and informed about the magnetosphere as the Earth's protective shield. The program included several magnetometry experiments, computer games, a children's corner, a remote controlled Mars Rover tour, a stage discussion and last but not least a "How to cook a comet" show.

On 13 November, an "Einstein-Junior" families' afternoon was organized at IWF. About 30 children (Fig. 41) and their parents learned about *Rosetta* and *Philae* on their way to comet 67P/CG. The program included several movie shows, a guided tour through the cometary lab, a "How to cook a comet" show, and a finishing quiz, where the young space experts answered easily even the most difficult questions. The celebratory end of this afternoon was the night launch of two water rockets.

Fig. 41: Children participating in the "Einstein-Junior" families' afternoon at IWF.

From 23-26 November, a "Post Alpbach" meeting was held at Schloss St. Martin, where Günter Kargl served as tutor.

During summer time, six high-school students performed an internship at IWF under the "Talente-Praktika" program of FFG. They worked on *MMS* data calibration, cometary dust and *MIDAS*, El Niño from space, a miniaturized magnetic field instrument, VLF wave propagation, and the geophysics/meteorology of the Novara expedition.

Throughout the rest of the year, many different groups and school classes visited the institute and were guided through the labs and the planetary garden.

AWARDS & RECOGNITION

For his successful public outreach work, especially in the context of the *Rosetta* mission, IWF director Wolfgang Baumjohann was named "scientist of the year" 2014 by the Austrian Club of Education and Science Journalists (Fig. 42). On 31 January, he was invited as guest of honor to the Vienna Ball of Sciences held in Vienna's townhall.

MEETINGS

Wolfgang Baumjohann served as Vice Director and on the Program Committee of the Summer School Alpbach, which took place from 14 to 23 July and was dedicated to „Quan-

tum Physics and Fundamental Physics in Space". Every year, 60 students and about 25 lecturers and tutors from among ESA's member states are invited to this meeting.

Additionally, H. Lammer and M. Scherf were members of program and/or scientific organizing committees for three international conferences and/or workshops.

T. Al-Ubaidi, M. Andriopoulou, M.Y. Boudjada, G. Kargl, M.L. Khodachenko, G. Kirchner, H. Lammer, C. Möstl, R. Nakamura, G. Stangl, and M. Volwerk organized or chaired 18 sessions at 7 international meetings.

Fig. 42: Chairman Oliver Lehmann congratulated Wolfgang Baumjohann (Photo: R. Ferrigato).

LECTURING

In summer 2015 and in winter term 2015/2016 IWF members gave lectures at the University of Graz, Graz University of Technology, University of Vienna, TU Braunschweig, FH Joanneum, and FH Wiener Neustadt.

THESES

Besides lecturing, members of the institute are supervising Bachelor, Diploma, Master and Doctoral Theses. In 2015, the following supervised theses have been completed:

Juvan, I.: Exoplanet Transit Light Curve Study and Analysis Concerning Star-Planet Interactions and Exomoons, Master Thesis, Universität Graz, 75 pages (2015)

Pfannekuche, M.: Charakterisierung von Spektralprofilen in thermisch getriebenen Sternwinden, Bachelor Thesis, TU Braunschweig, 47 pages (2015)

Purkhauser, A.: On the Use of Doppler Measurements for Dynamic Orbit Computation. Case Study: GRAIL, Master Thesis, Technische Universität Graz, 58 pages (2015)

Reimond, St.: Representation of the Gravity Field of Irregularly Shaped Bodies, Master Thesis, Technische Universität Graz, 72 pages (2015)

PUBLICATIONS

REFEREED ARTICLES

Alexandrova, A., R. Nakamura, V.S. Semenov, T.K.M. Nakamura: Motion of reconnection region in the Earth's magnetotail, *Geophys. Res. Lett.*, **42**, 4685-4693 (2015)

Ammler von Eiff, M., D. Sebastian, E.W. Guenther, B. Stecklum, J. Cabrera: The power of low-resolution spectroscopy: On the spectral classification of planet candidates in the ground-based CoRoT follow-up, *Astron. Nachr.*, **336**, 134-144 (2015)

Andriopoulou, M., R. Nakamura, K. Torkar, W. Baumjohann, B. Hoelzl: Deriving plasma densities in tenuous plasma regions, with the spacecraft potential under active control, *J. Geophys. Res.*, **120**, 9594-9616 (2015)

Appourchaux, T., H.M. Antia, W. Ball, O. Creevey, Y. Lebreton, K. Verma, S. Vorontsov, T.L. Campante, G.R. Davies, P. Gaulme, C. Régulo, E. Horch, S. Howell, M. Everett, D. Ciardi, L. Fossati, A. Miglio, J. Montalbán, W.J. Chaplin, R. A. García, L. Gizon: A seismic and gravitationally bound double star observed by Kepler. Implication for the presence of a convective core, *Astron. Astrophys.*, **582**, A25 (2015)

Archer, M.O., F. Plaschke: What frequencies of standing surface waves can the subsolar magnetopause support?, *J. Geophys. Res.*, **120**, 3632-3646 (2015)

Archer, M.O., M.D. Hartinger, B.M. Walsh, F. Plaschke, V. Angelopoulos: Frequency variability of standing Alfvén waves excited by fast mode resonances in the outer magnetosphere, *Geophys. Res. Lett.*, **42**, 10150-10159 (2015)

Arkhypov, O.V., M.L. Khodachenko, H. Lammer, M. Güdel, Th. Lüftinger, C.P. Johnstone: Short-period stellar activity cycles with Kepler photometry, *Astrophys. J.*, **807**, 109 (2015)

Arkhypov, O.V., M.L. Khodachenko, M. Güdel, C. Johnstone, T. Lüftinger, H. Lammer: Signs of deep mixing in starspot variability, *Astron. Astrophys.*, **576**, A67 (2015)

Artemyev, A.V., A.A. Petrukovich, R. Nakamura, L.M. Zelenyi: Statistics of intense dawn-dusk currents in the Earth's magnetotail, *J. Geophys. Res.*, **120**, 3804-3820 (2015)

Artemyev, A.V., A.A. Petrukovich, R. Nakamura, L.M. Zelenyi: Two-dimensional configuration of the magnetotail current sheet: THEMIS observations, *Geophys. Res. Lett.*, **42**, 3662-3667 (2015)

Auster, H.-U., I. Apathy, G. Berghofer, K.-H. Fornacon, A. Remizov, Ch. Carr, C. Güttler, G. Haerendel, Ph. Heinisch, D. Hercik, M. Hilchenbach, E. Kührt, W. Magnes, U. Motschmann, I. Richter, Ch.T. Russell, A. Przyklenk, K. Schwingenschuh, H. Sierks, K.-H. Glassmeier: The nonmagnetic nucleus of comet 67P/Churyumov-Gerasimenko, *Science*, **349**, aaa5102 (2015)

Bagnulo, S., L. Fossati, J.D. Landstreet, C. Izzo: The FORS1 catalogue of stellar magnetic fields, *Astron. Astrophys.*, **583**, A115 (2015)

Biele, J., St. Ulamec, M. Maibaum, R. Roll, L. Witte, E. Jurado, P. Muñoz, W. Arnold, H.-U. Auster, C. Casas, C. Faber, C. Fantinati, F. Finke, H.-H. Fischer, K. Geurts, C. Güttler, Ph. Heinisch, A. Herique, St. Hviid, G. Kargl, M. Knappmeyer, J. Knollenberg, W. Kofman, N. Kömle, E. Kührt, V. Lommatsch, St. Mottola, R.P. de Santayana, E. Remetean, F. Scholten, K.J. Seidensticker, H. Sierks, T. Spohn: The landing(s) of Philae and inferences about comet surface mechanical properties, *Science*, **349**, aaa9816 (2015)

Bocanegra-Bahamon, T., C. Bracken, M.C. Sitja, D. Dirkx, I. Gerth, K. Konstantinidis, Ch. Labrianidis, M. Laneuville, A. Luntzer, J.L. MacArthur, A. Maier, A. Morschhauser, T.A. Nordheim, R. Sallantin, R. Tlustos: MUSE - Mission to the Uranian system: Unveiling the evolution and formation of ice giants, *Adv. Space Res.*, **55**, 2190-2216 (2015)

Bourdin, P.A., S. Bingert, H. Peter: Coronal energy input and dissipation in a solar active region 3D MHD model, *Astron. Astrophys.*, **580**, A72 (2015)

Bunescu, C., O. Marghitu, D. Constantinescu, Y. Narita, J. Vogt, A. Blagau: Multiscale field-aligned current analyzer, *J. Geophys. Res.*, **120**, 9563-9577 (2015)

Cabrera, J., Sz. Csizmadia, G. Montagnier, M. Fridlund, M. Ammler-von Eiff, S. Chaintreuil, C. Damiani, M. Deleuil, S. Ferraz-Mello, A. Ferrigno, D. Gandolfi, T. Guillot, E.W. Guenther, A. Hatzes, G. Hébrard, P. Klagyivik, H. Parviainen, Th. Pasternacki, M. Pätzold, D. Sebastian, M. Tadeu dos Santos, G. Wuchterl, S. Aigrain, R. Alonso, J.-M. Almenara, J.D. Armstrong, M. Auvergne, A. Baglin, P. Barge, S.C.C. Barros, A.S. Bonomo, P. Bordé, F. Bouchy, S. Carpano, C. Chaffey, H.J. Deeg, R.F.Díaz, R. Dvorak, A. Erikson, S. Grziwa, J. Korth, H. Lammer, C. Lindsay, T. Mazeh, C. Moutou, A. Ofir, M. Ollivier, E. Pallé, H. Rauer, D. Rouan, B. Samuel, A. Santerne, J. Schneider: Transiting exoplanets from the CoRoT space mission. XXVII. CoRoT-28b, a planet orbiting an evolved star, and CoRoT-29b, a planet showing an asymmetric transit, *Astron. Astrophys.*, **579**, A36 (2015)

Chai, L., W. Wan, M. Fraenz, T.L. Zhang, E. Dubinin, Y. Wei, Y. Li, Z. Rong, J. Zhong, X. Han, Y. Futaana: Solar zenith angle-dependent asymmetries in Venusian bow shock location revealed by Venus Express, *J. Geophys. Res.*, **120**, 4446-4452 (2015)

Collinson, G.A., J. Grebowsky, D.G. Sibeck, L.K. Jian, S. Boardsen, J. Espley, D. Hartle, T.L. Zhang, St. Barabash, Y. Futaana, P. Kollmann: The impact of a slow interplanetary coronal mass ejection on Venus, *J. Geophys. Res.*, **120**, 3489-3502 (2015)

Comisel, H., U. Motschmann, J. Büchner, Y. Narita, Y. Nariyuki: Ion-scale turbulence in the inner heliosphere: Radial dependence, *Astrophys. J.*, **812**, 175 (2015)

Comisel, H., Y. Narita, U. Motschmann: Adaptation of the de Hoffmann-Teller frame for quasi-perpendicular collisionless shocks, *Ann. Geophys.*, **33**, 345-350 (2015)

Comisel, H., Y. Narita, U. Motschmann: Dispersion relation as a channel of plasma turbulence evolution, *Earth Planets Space*, **67**, 32 (2015)

Delva, M., C. Bertucci, M. Volwerk, R. Lundin, C. Mazelle, N. Romanelli: Upstream proton cyclotron waves at Venus near solar maximum, *J. Geophys. Res.*, **120**, 344-354 (2015)

Dorovskyy, V.V., V.N. Melnik, A.A. Konovalenko, A.I. Brazhenko, M. Panchenko, S. Poedts,V.A. Mykhaylov: Fine and superfine structure of the decameter–hectometer type II burst on 7 June 2011, *Solar Phys.*, **290**, 2031-2042 (2015)

Dorovskyy, V.V., V.N. Melnik, A.A. Konovalenko, I.N. Bubnov, A.A. Gridin, N.V. Shevchuk, H.O. Rucker, S. Poedts, M. Panchenko: Decameter U-burst harmonic pair from a high loop, *Solar Phys.*, **290**, 181-192 (2015)

Dwivedi, N.K., D. Schmid, Y. Narita, P. Kovacs, Z. Vörös, M. Delva, T.L. Zhang: Statistical investigation on the power-law behavior of magnetic fluctuations in the Venusian magnetosheath, *Earth Planets Space*, **67**, 137 (2015)

Edberg, N.J.T., A.I. Eriksson, E. Odelstad, P. Henri, J.-P. Lebreton, S. Gasc, M. Rubin, M. André, R. Gill, E.P.G. Johansson, F. Johansson, E. Vigren, J.E. Wahlund, C.M. Carr, E. Cupido, K.-H. Glassmeier, R. Goldstein, C. Koenders, K. Mandt, Z. Nemeth, H. Nilsson, I. Richter, G. Stenberg Wieser, K. Szego, M. Volwerk: Spatial distribution of low-energy plasma around comet 67P/CG from Rosetta measurements, *Geophys. Res. Lett.*, **42**, 4263-4269 (2015)

Erkaev, N.V., H. Lammer, P. Odert, Yu.N. Kulikov, K.G. Kislyakova: Extreme hydrodynamic atmospheric loss near the critical thermal escape regime, *MNRAS*, **448**, 1916-1921 (2015)

Fischer, G., D.A. Gurnett, W.S. Kurth, S.-Y. Ye, J.B. Groene: Saturn kilometric radiation periodicity after equinox, *Icarus*, **254**, 72-91 (2015)

Fossati, L., K. France, T. Koskinen, I.G. Juvan, C.A. Haswell, M. Lendl: Far-uv spectroscopy of the planet-hosting star WASP-13: High-energy irradiance, distance, age, planetary mass-loss rate, and circumstellar environment, *Astrophys. J.*, **815**, 118 (2015)

Fossati, L., N. Castro, M. Schöller, S. Hubrig, N. Langer, T. Morel, M. Briquet, A. Herrero, N. Przybilla, H. Sana, F.R.N. Schneider, A. de Koter, BOB Collaboration: B fields in OB stars (BOB): Low-resolution FORS2 spectropolarimetry of the first sample of 50 massive stars, *Astron. Astrophys.*, **582**, A45 (2015)

Fossati, L., S. Ingrassia, A.F. Lanza: A bimodal correlation between host star chromospheric emission and the surface gravity of hot Jupiters, *Astrophys. J. Lett.*, **812**, L35 (2015)

Grassitelli, L., L. Fossati, N. Langer, A. Miglio, A.G. Istrate, D. Sanyal: Relating turbulent pressure and macroturbulence across the HR diagram with a possible link to \gamma Doradus stars, *Astron. Astrophys.*, **584**, L2 (2015)

Grassitelli, L., L. Fossati, S. Simón-Diáz, N. Langer, N. Castro, D. Sanyal: Observational consequences of turbulent pressure in the envelops of massive stars, *Astrophys. J. Lett.*, **808**, L31 (2015)

Hartinger, M.D., F. Plaschke, M.O. Archer, D.T. Welling, M.B. Moldwin, A. Ridley: The global structure and time evolution of dayside magnetopause surface eigenmodes, *Geophys. Res. Lett.*, **42**, 2594-2602 (2015)

Hasegawa, H., B.U.Ö. Sonnerup, S. Eriksson, T.K.M. Nakamura, H. Kawano: Dual-spacecraft reconstruction of a three-dimensional magnetic flux rope at the Earth's magnetopause, *Ann. Geophys.*, **33**, 169-184 (2015)

Hettrich, S., Y. Kempf, N. Perakis, J. Gorski, M. Edl, J. Urbar, M. Dosa, F. Gini, O.W. Roberts, St. Schindler, M. Schemmer, D. Steenari, N. Joldzic, L.-K. Glesnes Odegaard, D. Sarria, M. Volwerk, J. Praks: Atmospheric Drag, Occultation 'N' Ionospheric Scintillation (ADONIS) mission proposal, *J Space Weather Space Clim*, **5**, A2 (2015)

Jackman, C.M., M.F. Thomsen, D.G. Mitchell, N. Sergis, C.S. Arridge, M. Felici, S.V. Badman, C. Paranicas, X. Jia, G.B. Hospodarksy, M. Andriopoulou, K.K. Khurana, A.W. Smith, M.K. Dougherty: Field dipolarization in Saturn's magnetotail with planetward ion flows and energetic particle flow bursts: Evidence of quasi-steady reconnection, *J. Geophys. Res.*, **120**, 3603-3617 (2015)

Johnstone, C.P., M. Güdel, A. Stökl, H. Lammer, L. Tu, K.G. Kislyakova, T. Lüftinger, P. Odert, N.V. Erkaev, E.A. Dorfi: The evolution of stellar rotation and the hydrogen atmospheres of habitable-zone terrestrial planets, *Astrophys. J. Lett.*, **815**, L12 (2015)

Kepko, L., R.L. McPherron, O. Amm, S. Apatenkov, W. Baumjohann, J. Birn, M. Lester, R. Nakamura, T.I. Pulkkinen, V. Sergeev: Substorm current wedge revisited, *Space Sci. Rev.*, **190**, 1-46 (2015)

Khodachenko, M.L., I.F. Shaikhislamov, H. Lammer, P.A. Prokopov: Atmosphere expansion and mass loss of close-orbit giant exoplanets heated by stellar XUV. II. Effects of planetary magnetic field; structuring of inner magnetosphere, *Astrophys. J.*, **813**, 50 (2015)

Kislyakova, K.G., L. Fossati, C.P. Johnstone, M. Holmström, V.V. Zaitsev, H. Lammer: Stellar wind induced soft x-ray emission from close-in exoplanets, *Astrophys. J. Lett.*, **799**, L15, (2015)

Kömle, N.I., J. Poganski, G. Kargl, J. Grygorczuk: Pile driving models for the evaluation of soil penetration resistance measurements from planetary subsurface probes, *Planet. Space Sci.*, **109-110**, 135-148 (2015)

Korovinskiy, D.B., A.V. Divin, N.V. Erkaev, V.S. Semenov, A.V. Artemyev, V.V. Ivanova, I.B. Ivanov, G. Lapenta, S. Markidis, H.K. Biernat: The double-gradient magnetic instability: Stabilizing effect of the guide field, *Phys. Plasmas*, **22**, 012904 (2015)

Krauss, S., M. Temmer, A. Veronig, O. Baur, H. Lammer: Thermospheric and geomagnetic responses to interplanetary coronal mass ejections observed by ACE and GRACE: Statistical results, *J. Geophys. Res.*, **120**, 8848-8860 (2015)

Kucharski, D., G. Kirchner, T. Otsubo, F. Koidl: A method to calculate zero-signature satellite laser ranging normal points for millimeter geodesy - a case study with Ajisai, *Earth Planets Space*, **67**, 34 (2015)

Kumar, S., N.K. Dwivedi, R.P. Sharma, Y.-J. Moon: Numerical study of density cavitations by inertial Alfvén waves, *Astrophys. Space Sci.*, **358**, 5 (2015)

Kuridze, D., V. Henriques, M. Mathioudakis, R. Erdélyi, T.V. Zaqarashvili, S. Shelyag, P.H. Keys, F.P. Keenan: The dynamics of rapid redshifted and blueshifted excursions in the solar Hα line, *Astrophys. J.*, **802**, 26 (2015)

Leconte, J., F. Forget, H. Lammer: On the (anticipated) diversity of terrestrial planet atmospheres, *Exp. Astron.*, **40**, 449-467 (2015)

Leitner, S., A. Valavanoglou, P. Brown, C. Hagen, W. Magnes, B.J. Whiteside, C.M. Carr, M. Delva, W. Baumjohann: Design of the magnetoresistive magnetometer for ESA's SOSMAG project, *IEEE Trans. Magnetics*, **51**, 40011404 (2015)

Lhotka, C.: Sitnikov's planet, *Rivista dell'UMI*, **Ser I, 8**, 1-31 (2015)

Lhotka, C., A. Celletti: The effect of Poynting-Robertson drag on the triangular Lagrangian points, *Icarus*, **250**, 249-261 (2015)

Lu, H.Y., J.B. Cao, T.L. Zhang, H.S. Fu, Y.S. Ge: Evolution of Kelvin-Helmholtz instability at Venus in the presence of the parallel magnetic field, *Phys. Plasmas*, **22**, 062902 (2015)

Lu, H.Y., J.B. Cao, Y.S. Ge, T.L. Zhang, R. Nakamura, M.W. Dunlop: Hall and finite Larmor radius effects on the dipolarization fronts associated with interchange instability, *Geophys. Res. Lett.*, **42**, 10099-10105 (2015)

Luhmann, J.G., Y.J. Ma, M.N. Villarreal, H.Y. Wei, T.L. Zhang: The Venus-solar wind interaction: Is it purely ionospheric?, *Planet. Space Sci.*, **119**, 36-42 (2015)

Mackey, J., N. Castro, L. Fossati, N. Langer: Cold gas in hot star clusters: The wind from the red supergiant W26 in Westerlund 1, *Astron. Astrophys.*, **582**, A24 (2015)

Maindl, T.I., R. Dvorak, H. Lammer, M. Güdel, C. Schäfer, R. Speith, P. Odert, N.V. Erkaev, K.G. Kislyakova, E. Pilat-Lohinger: Impact induced surface heating by planetesimals on early Mars, *Astron. Astrophys.*, **574**, A22 (2015)

Marsch, E., Y. Narita: Fermion unification model based on the intrinsic SU(8) symmetry of a generalized Dirac equation, *Front. Physics*, **3**, 82 (2015)

Masunaga, K., K. Seki, N. Terada, F. Tsuchiya, T. Kimura, K. Yoshioka, G. Murakami, A. Yamazaki, M. Kagitani, C. Tao, A. Fedorov, Y. Futaana, T.L. Zhang, D. Shiota1, F. Leblanc, J.-Y. Chaufray, I. Yoshikawa: Periodic variations of oxygen EUV dayglow in the upper atmosphere of Venus: Hisaki/EXCEED observations, *J. Geophys. Res.*, **120**, 2037-2052 (2015)

Mays, M.L., B.J. Thompson, L.K. Jian, R.C. Colaninno, D. Odstrcil, C. Möstl, M. Temmer, N.P. Savani, G. Collinson, A. Taktakishvili, P.J. MacNeice, Y. Zheng: Propagation of the 2014 January 7 CME and resulting geomagnetic non-event, *Astrophys. J.*, **812**, 145 (2015)

Melnik, V.N., A.I. Brazhenko, A.A. Konovalenko, C. Briand, V.V. Dorovskyy, P. Zarka, A.V. Frantsuzenko, H.O. Rucker, B.P. Rutkevych, M. Panchenko, L. Denis, T. Zaqarashvili, B. Shergelashvili: Decameter type III bursts with changing frequency drift-rate signs, *Solar Phys.*, **290**, 193-203 (2015)

Mghebrishvili, I., T.V. Zaqarashvili, V. Kukhianidze, G. Ramishvili, B. Shergelashvili, A. Veronig, St. Poedts: Dynamics of a solar prominence tornado observed by SDO/AIA on 2012 November 7-8, *Astrophys. J.*, **810**, 89 (2015)

Möstl, C., T. Rollett, R.A. Frahm, Y.D. Liu, D.M. Long, R.C. Colaninno, M.A. Reiss, M. Temmer, Ch.J. Farrugia, A. Posner, M. Dumbovic, M. Janvier, P. Demoulin, P. Boakes, A. Devos, E. Kraaikamp, M.L. Mays, B. Vrsnak: Strong coronal channelling and interplanetary evolution of a solar storm up to Earth and Mars, *Nat. Comm.*, **6**, 7135 (2015)

Narita, Y.: Non-elliptic wavevector anisotropy for magnetohydrodynamic turbulence, *Ann. Geophys.*, **33**, 1413-1419 (2015)

Narita, Y., E. Marsch: Kinetic slow mode in the solar wind and its possible role in turbulence dissipation and ion heating, *Astrophys. J.*, **805**, 24 (2015)

Nilsson, H., G. Stenberg Wieser, E. Behar, C. Simon Wedlund, E. Kallio, H. Gunell, N.J.T. Edberg, A.I. Eriksson, M. Yamauchi, C. Koenders, M. Wieser, R. Lundin, S. Barabash, K. Mandt, J.L. Burch, R. Goldstein, P. Mokashi, C. Carr, E. Cupido, P.T. Fox, K. Szego, Z. Nemeth, A. Fedorov, J.-A. Sauvaud, H. Koskinen, I. Richter, J.-P. Lebreton, P. Henri, M. Volwerk, C. Vallat, B. Geiger: Evolution of the ion environment of comet 67P/Churyumov-Gerasimenko. Observations between 3.6 and 2.0 AU, *Astron. Astrophys.*, **583**, A20 (2015)

Nilsson, H., G. Stenberg Wieser, E. Behar, C.S. Wedlund, H. Gunell, M. Yamauchi, R. Lundin, S. Barabash, M. Wieser, C. Carr, E. Cupido, J.L. Burch, A. Fedorov, J.-A. Sauvaud, H. Koskinen, E. Kallio, J.-P. Lebreton, A. Eriksson, N. Edberg, R. Goldstein, P. Henri, C. Koenders, P. Mokashi, Z. Nemeth, I. Richter, K. Szego, M. Volwerk, C. Vallat, M. Rubin: Birth of a comet magnetosphere: A spring of water ions, *Science*, **347**, aaa0571 (2015)

Palin, L., C. Jacquey, H. Opgenoorth, M. Connors, V. Sergeev, J.-A. Sauvaud, R. Nakamura, G.D. Reeves, H.J. Singer, V. Angelopoulos, L. Turc: Three-dimensional current systems and ionospheric effects associated with small dipolarization fronts, *J. Geophys. Res.*, **120**, 3739-3757 (2015)

Panov, E.V., R.A. Wolf, M.V. Kubyshkina, R. Nakamura, W. Baumjohann: Anharmonic oscillatory flow braking in the Earth's magnetotail, *Geophys. Res. Lett.*, **42**, 3700-3706 (2015)

Petermann, I., N. Langer, N. Castro, L. Fossati: Blue supergiants as descendants of magnetic main sequence stars, *Astron. Astrophys.*, **584**, A54 (2015)

Petrukovich, A., A. Artemyev, R. Nakamura, L. Zelenyi: Current sheets in the Earth magnetotail: Plasma and magnetic field structure with Cluster project observations, *Space Sci. Rev.*, **188**, 311-337 (2015)

Pfleger, M., H.I.M. Lichtenegger, P. Wurz, H. Lammer, E. Kallio, M. Alho, A. Mura, S. McKenna-Lawlor, J.A. Martín-Fernández: 3D-modeling of Mercury's solar wind sputtered surface-exosphere environment, *Planet. Space Sci.*, **115**, 90-101 (2015)

Plainaki, C., M. Laurenza, H. Mavromichalaki, M. Storini, M. Gerontidou, A. Kanellakopoulos, M. Andriopoulou, A. Belov, E. Eroshenko, V. Yanke: Derivation of relativistic SEP properties through neutron monitor data modeling, *J. Phys. Conf. Ser.*, **632**, 012076 (2015)

Richter, I., C. Koenders, H.-U. Auster, D. Frühauff, C. Götz, P. Heinisch, C. Perschke, U. Motschmann, B. Stoll, K. Altwegg, J. Burch, C. Carr, E. Cupido, A. Eriksson, P. Henri, R. Goldstein, J.-P. Lebreton, P. Mokashi, Z. Nemeth, H. Nilsson, M. Rubin, K. Szegö, B.T. Tsurutani, C. Vallat, M. Volwerk, K.-H. Glassmeier: Observation of a new type of low-frequency waves at comet 67P/Churyumov-Gerasimenko, *Ann. Geophys.*, **33**, 1031-1036 (2015)

Rong, Z.J., A.T.Y. Lui, W.X. Wan, Y.Y. Yang, C. Shen, A.A. Petrukovich, Y.C. Zhang, T.L. Zhang, Y. Wei: Time delay of interplanetary magnetic field penetration into Earth's magnetotail, *J. Geophys. Res.*, **120**, 3406-3414 (2015)

Rong, Z.J., S. Barabash, G. Stenberg, Y. Futaana, T.L. Zhang, W.X. Wan, Y. Wei, X.-D. Wang: Technique for diagnosing the flapping motion of magnetotail current sheets based on single-point magnetic field analysis, *J. Geophys. Res.*, **120**, 3462-3474 (2015)

Rong, Z.J., S. Barabash, G. Stenberg, Y. Futaana, T.L. Zhang, W.X. Wan, Y. Wei, X.D. Wang, L.H. Chai, J. Zhong: The flapping motion of the Venusian magnetotail: Venus Express observations, *J. Geophys. Res.*, **120**, 5593-5602 (2015)

Rozhnoi, A., M. Solovieva, M. Parrot, M. Hayakawa, P.-F. Biagi, K. Schwingenschuh, V. Fedun: VLF/LF signal studies of the ionospheric response to strong seismic activity in the Far Eastern region combining the DEMETER and ground-based observations, *Phys. Chem. Earth*, **85-86**, 141-149 (2015)

Sampl, M., W. Macher, C. Gruber, T. Oswald, M. Kapper, H.O. Rucker, M. Mogilevsky: High-frequency performance of electric field sensors aboard the RESONANCE satellite, *Geosci. Instrum. Method. Data Syst.*, **4**, 81-88 (2015)

Sansottera, M., Ch. Lhotka, A. Lemaitre: Effective resonant stability of Mercury, *MNRAS*, **452**, 4145-4152 (2015)

Sasunov, Yu.L., M.L. Khodachenko, I.I. Alexeev, E.S. Belenkaya, E.I. Gordeev, I.V. Kubyshkin: The energy-based scaling of a thin current sheet: Case study, *Geophys. Res. Lett.*, **42**, 9609-9616 (2015)

Sasunov, Yu.L., M.L. Khodachenko, I.I. Alexeev, E.S. Belenkaya, V.S. Semenov, I.V. Kubyshkin, O.V. Mingalev: Investigation of scaling properties of a thin current sheet by means of particle trajectories study, *J. Geophys. Res.*, **120**, 1633-1645 (2015)

Sasunov, Yu.L., V.S. Semenov, M.F. Heyn, N.V. Erkaev, I.V. Kubyshkin, K.Yu. Slivka, D.B. Korovinskiy, M.L. Khodachenko: A statistical survey of reconnection exhausts in the solar wind based on the Riemannian decay of current sheets, *J. Geophys. Res.*, **120**, 8194-8209 (2015)

Schmid, D., R. Nakamura, F. Plaschke, M. Volwerk, W. Baumjohann: Two states of magnetotail dipolarization fronts: A statistical study, *J. Geophys. Res.*, **120**, 1096-1108 (2015)

Shan, L., Q. Lu, Ch. Mazelle, C. Huang, T.L. Zhang, M. Wu, X. Gao, S. Wang: The shape of the Venusian bow shock at solar minimum and maximum: Revisit based on VEX observations, *Planet. Space Sci.*, **109-110**, 32-37 (2015)

Slivka, K.Yu., V.S. Semenov, N.V. Erkaev, N.P. Dmitrieva, I.V. Kubyshkin, H. Lammer: Peculiarities of magnetic barrier formation for southward and northward directions of the IMF, *J. Geophys. Res.*, **120**, 9471-9483 (2015)

Soler, R., J.L. Ballester, T.V. Zaqarashvili: Overdamped Alfvén waves due to ion-neutral collisions in the solar chromosphere, *Astron. Astrophys.*, **573**, A79 (2015)

Solovieva, M., A. Rozhnoi, V. Fedun, K. Schwingenschuh, M. Hayakawa: Ionospheric perturbations related to the earthquake in Vrancea area on November 22, 2014, as detected by electromagnetic VLF/LF frequency signals, *Ann. of Geophys.*, **58**, A0552 (2015)

Spohn, T., J. Knollenberg, A.J. Ball, M. Banaszkiewicz, J. Benkhoff, M. Grott, J. Grygorczuk, C. Hüttig, A. Hagermann, G. Kargl, E. Kaufmann, N. Kömle, E. Kührt, K. J. Kossacki, W. Marczewski, I. Pelivan, R. Schrödter, K. Seiferlin: Thermal and mechanical properties of the near-surface layers of comet 67P/Churyumov-Gerasimenko, *Science*, **349**, aaa0464 (2015)

Stanislavsky, A.A., A.A. Konovalenko, A.A. Koval, V.V. Dorovskyy, P. Zarka, H.O. Rucker: Coronal magnetic field strength from decameter zebra-pattern observations: Complementarity with band-splitting measurements of an associated type II burst, *Solar Phys.*, **290**, 205-218 (2015)

Stenberg Wieser, G., M. Ashfaque, H. Nilsson, Y. Futaana, S. Barabash, C. Diéval, A. Fedorov, T.L. Zhang: Proton and alpha particle precipitation on to the upper atmosphere of Venus, *Planet. Space Sci.*, **113-114**, 369-377 (2015)

Stökl, A., E. Dorfi, H. Lammer: Hydrodynamic simulations of captured protoatmospheres around Earth-like planets, *Astron. Astrophys.*, **576**, A87 (2015)

Strugarek, A., N. Janitzek, A. Lee, Ph. Lösch, B. Seifert, S. Hoilijoki, E. Kraaikamp, A.I. Mrigakshi, T. Philippe, S. Spina, M. Bröse, S. Massahi, L. O'Halloran, V. Pereira Blanco, Ch. Stausland, Ph. Escoubet, G. Kargl: A Space Weather mission concept: Observatories of the Solar Corona and Active Regions (OSCAR), *J Space Weather Space Clim*, **5**, A4 (2015)

Teh, W.-L., T.K.M. Nakamura, R. Nakamura, W. Baumjohann, M. Abdullah: On the evolution of a magnetic flux rope: Two-dimensional MHD simulation results, *J. Geophys. Res.*, **120**, 8547-8558 (2015)

Teodorescu, E., M. Echim, C. Munteanu, T.-L. Zhang, R. Bruno, P. Kovacs: Inertial range turbulence of fast solar wind at 0.72 AU and solar minimum, *Astrophys. J. Lett.*, **804**, L41 (2015)

Tinetti, G., P. Drossart, P. Eccleston, P. Hartogh, K. Isaak, M. Linder, C. Lovis, G. Micela, M. Ollivier, L. Puig, I. Ribas, I. Snellen, B. Swinyard, F. Allard, J. Barstow, J. Cho, A. Coustenis, C. Cockell, A. Correia, L. Decin, R. de Kok, P. Deroo, T. Encrenaz, F. Forget, A. Glasse, C. Griffith, T. Guillot, T. Koskinen, H. Lammer, J. Leconte, P. Maxted, I. Mueller-Wodarg, R. Nelson, C. North, E. Pallé, I. Pagano, G. Piccioni, D. Pinfield, F. Selsis, A. Sozzetti, L. Stixrude, J. Tennyson, D. Turrini, M. Zapatero-Osorio, J.-P. Beaulieu, D. Grodent, M. Guedel, D. Luz, H.U. Norgaard-Nielsen, T. Ray, H. Rickman, A. Selig, M. Swain, M. Banaszkiewicz, M. Barlow, N. Bowles, G. Branduardi-Raymont, V. Coudé du Foresto, J.-C. Gerard, L. Gizon, A. Hornstrup, C. Jarchow, F. Kerschbaum, G. Kovacs, P.-O. Lagage, T. Lim, M. Lopez-Morales, G. Malaguti, E. Pace, E. Pascale, B. Vandenbussche, G. Wright, G.R. Zapata, A. Adriani, R. Azzollini, A. Balado, I. Bryson, R. Burston, J. Colomé, M. Crook, A. Di Giorgio, M. Griffin, R. Hoogeveen, R. Ottensamer, R. Irshad, K. Middleton, G. Morgante, F. Pinsard, M. Rataj, J.-M. Reess, G. Savini, J.-R. Schrader, R. Stamper, B. Winter, L. Abe, M. Abreu, N. Achilleos, P. Ade, V. Adybekian, L. Affer, C. Agnor, M. Agundez, C. Alard, J. Alcala, C. Allende Prieto, F.J. Alonso Floriano, F. Altieri, C.A. Alvarez Iglesias, P. Amado, A. Andersen, A. Aylward, C. Baffa, G. Bakos, P. Ballerini, M. Banaszkiewicz, R.J. Barber, D. Barrado, E.J. Barton, V. Batista, G. Bellucci, J.A. Belmonte Avilés, D. Berry, B. Bézard, D. Biondi, M. Błęcka, I. Boisse, B. Bonfond, P. Bordé, P. Börner, H. Bouy, L. Brown, L. Buchhave, J. Budaj, A. Bulgarelli, M. Burleigh, A. Cabral, M.T. Capria, A. Cassan, C. Cavarroc, C. Cecchi-Pestellini, R. Cerulli, J. Chadney, S. Chamberlain, S. Charnoz, N. Christian Jessen, A. Ciaravella, A. Claret, R. Claudi, A. Coates, R. Cole, A. Collura, D. Cordier, E. Covino, C. Danielski, M. Damasso, H. J. Deeg, E. Delgado-Mena, C. Del Vecchio, O. Demangeon, A. De Sio, J. De Wit, M. Dobrijévic, P. Doel, C. Dominic, E. Dorfi, S. Eales, C. Eiroa, M. Espinoza Contreras, M. Esposito, V. Eymet, N. Fabrizio, M. Fernández, B. Femenía Castella, P. Figueira, G. Filacchione, L. Fletcher, M. Focardi, S. Fossey, P. Fouqué, J. Frith, M. Galand, L. Gambicorti, P. Gaulme, R.J. García López, A. Garcia-Piquer, W. Gear, J.-C. Gerard, L. Gesa, E. Giani, F. Gianotti, M. Gillon, E. Giro, M. Giuranna, H. Gomez, I. Gomez-Leal, J. Gonzalez Hernandez, B. González Merino, R. Graczyk, D. Grassi, J. Guardia, P. Guio, J. Gustin, P. Hargrave, J. Haigh, E. Hébrard, U. Heiter, R. L. Heredero, E. Herrero, F. Hersant, D. Heyrovsky, M. Hollis, B. Hubert, R. Hueso, G. Israelian, N. Iro, P. Irwin, S. Jacquemoud, G. Jones, H. Jones, K. Justtanont, T. Kehoe, F. Kerschbaum, E. Kerins, P. Kervella, D. Kipping, T. Koskinen, N. Krupp, O. Lahav, B. Laken, N. Lanza, E. Lellouch, G. Leto, J. Licandro Goldaracena, C. Lithgow-Bertelloni, S.J. Liu, U. Lo Cicero, N. Lodieu, P. Lognonné, M. Lopez-Puertas, M. A. Lopez-Valverde, I. Lundgaard Rasmussen, A. Luntzer, P. Machado, C. MacTavish, A. Maggio, J.-P. Maillard, W. Magnes, J. Maldonado, U. Mall, J.-B. Marquette, P. Mauskopf, F. Massi, A.-S. Maurin, A. Medvedev, C. Michaut, P. Miles-Paez, M. Montalto, P. Montanés Rodríguez, M. Monteiro, D. Montes, H. Morais, J. C. Morales, M. Morales-Calderón, G. Morello, A. Moro Martín, J. Moses, A. Moya Bedon, F. Murgas Alcaino, E. Oliva, G. Orton, F. Palla, M. Pancrazzi, E. Pantin, V. Parmentier, H. Parviainen, K. Y. Pena Ramírez, J. Peralta, S. Perez-Hoyos, R. Petrov, S. Pezzuto, R. Pietrzak, E. Pilat-Lohinger, N. Piskunov, R. Prinja, L. Prisinzano, I. Polichtchouk, E. Poretti, A. Radioti, A. A. Ramos, T. Rank-Lüftinger, P. Read, K. Readorn, R. Rebolo López, J. Rebordão, M. Rengel, L. Rezac, M. Rocchetto, F. Rodler, V.J. Sánchez Béjar, A. Sanchez Lavega, E. Sanromá, N. Santos, J. Sanz Forcada, G. Scandariato, F.-X. Schmider, A. Scholz, S. Scuderi, J. Sethenadh, S. Shore, A. Showman, B. Sicardy, P. Sitek, A. Smith, L. Soret, S. Sousa, A. Stiepen, M. Stolarski, G. Strazzulla, H. M. Tabernero, P. Tanga, M. Tecsa, J. Temple, L. Terenzi, M. Tessenyi, L. Testi, S. Thompson, H. Thrastarson, B.W. Tingley, M. Trifoglio, J. Martín Torres, A. Tozzi, D. Turrini, R. Varley, F. Vakili, M. de Val-Borro, M. L. Valdivieso, O. Venot, E. Villaver, S. Vinatier, S. Viti, I. Waldmann, D. Waltham, D. Ward-Thompson, R. Waters, C. Watkins, D. Watson, P. Wawer, A. Wawrzaszk, G. White, T. Widemann, W. Winek, T. Wiśniowski, R. Yelle, Y. Yung, S. N. Yurchenko: The EChO science case, *Exp. Astron.*, **40**, 329-391 (2015)

Torkar, K., R. Nakamura, M. Andriopoulou: Interdependencies between the actively controlled Cluster spacecraft potential, ambient plasma, and electric field Measurements, *IEEE Trans. Plasma Sci.*, **43**, 3054-3063 (2015)

Treumann, R.A., W. Baumjohann: Broad current sheets, current bifurcation, and collisionless reconnection - An opinion on "Onset of fast magnetic reconnection via subcritical bifurcation" by Z.Guo and X.Wang, *Front. Physics*, **3**, 40 (2015)

Treumann, R.A., W. Baumjohann: Information kinetics - an extension, *Front. Physics*, **3**, 34 (2015)

Treumann, R.A., W. Baumjohann: Kinetic theory of information - the dynamics of information, *Front. Physics*, **3**, 19 (2015)

Treumann, R.A., W. Baumjohann: Spontaneous magnetic reconnection. Collisionless reconnection and its potential astrophysical relevance, *Astron. Astrophys. Rev.*, **23**, 4, (2015)

Treumann, R.A., W. Baumjohann, Y. Narita: Ideal MHD turbulence: The inertial range spectrum with collisionless dissipation, *Front. Physics*, **3**, 22 (2015)

Tu, L., C.P. Johnstone, M. Güdel, H. Lammer: The extreme ultraviolet and x-ray Sun in time: High-energy evolutionary tracks of a solar-like star, *Astron. Astrophys.*, **577**, L3 (2015)

Vashalomidze, Z., V. Kukhianidze, T.V. Zaqarashvili, R. Oliver, B. Shergelashvili, G. Ramishvili, S. Poedts, P. De Causmaecker: Formation and evolution of coronal rain observed by SDO/AIA on February 22, 2012, *Astron. Astrophys.*, **577**, A136 (2015)

Vasko, I.Y., A.A. Petrukovich, A.V. Artemyev, R. Nakamura, L.M. Zelenyi: Earth's distant magnetotail current sheet near and beyond lunar orbit, *J. Geophys. Res.*, **120**, 8663-8680 (2015)

Villarreal, M.N., C.T. Russell, H.Y. Wei, Y.J. Ma, J.G. Luhmann, R.J. Strangeway, T.L. Zhang: Characterizing the low-altitude magnetic belt at Venus: Complementary observations from the Pioneer Venus Orbiter and Venus Express, *J. Geophys. Res.*, **120**, 2232-2240 (2015)

Vorburger, A., P. Wurz, H. Lammer, S. Barabash, O. Mousis: Monte-Carlo simulation of Callisto's exosphere, *Icarus*, **262**, 14-29 (2015)

Vörös, Z., M. Leitner, Y. Narita, G. Consolini, P. Kovács, A. Tóth, J. Lichtenberger: Probability density functions for the variable solar wind near the solar cycle minimum, *J. Geophys. Res.*, **120**, 6152-6166 (2015)

Wang, Ch.-P., X. Xing, T.K.M. Nakamura, L.R. Lyons: Dawn-dusk asymmetry in bursty hot electron enhancements in the midtail magnetosheath, *J. Geophys. Res.*, **120**, 7228-7239 (2015)

Wang, G.Q., T.L. Zhang, Y.S. Ge: Spatial distribution of magnetic fluctuation power with period 40 to 600s in the magnetosphere observed by THEMIS, *J. Geophys. Res.*, **120**, 9281-9293 (2015)

Wang, G.Q., Y.S. Ge, T.L. Zhang, R. Nakamura, M. Volwerk, W. Baumjohann, A.M. Du, Q.M. Lu: A statistical analysis of Pi2-band waves in the plasma sheet and their relation to magnetospheric drivers, *J. Geophys. Res.*, **120**, 6167-6175 (2015)

Wang, J., A.M. Du, Y. Zhang, T.L. Zhang, Y.S. Ge: Modeling the Earth's magnetosphere under the influence of solar wind with due northward IMF by the AMR-CESE-MHD model, *Sci. China D*, **58**, 1235-1242 (2015)

Wang, Z., J.K. Shi, K. Torkar, G.J. Wang, X. Wang: A case study on ionospheric scintillations at low latitude associated with a plasma blob observed in situ, *Geophys. Res. Lett.*, **42**, 2109-2114 (2015)

Wedemeyer, S., T. Bastian, R. Brajsa, M. Barta, H. Hudson, G. Fleishman, M. Loukitcheva, B. Fleck, E. Kontar, B. De Pontieu, S. Tiwari, Y. Kato, R. Soler, P. Yagoubov, J.H. Black, P. Antolin, S. Gunar, N. Labrosse, A.O. Benz, A. Nindos, M. Steffen, E. Scullion, J.G. Doyle, T. Zaqarashvili, A. Hanslmeier, V.M. Nakariakov, P. Heinzel, T. Ayres, M. Karlicky, and the SSALMON Group: SSALMON - The Solar Simulations for the Atacama Large Millimeter Observatory Network, *Adv. Space Res.*, **56**, 2679-2692 (2015)

Wirnsberger, H., O. Baur, G. Kirchner: Space debris orbit prediction errors using bi-static laser observations. Case study: ENVISAT, *Adv. Space Res.*, **55**, 2607-2615 (2015)

Wu, M., C. Huang, Q. Lu, M. Volwerk, R. Nakamura, Z. Vörös, T.L. Zhang, S. Wang: In situ observations of multistage electron acceleration driven by magnetic reconnection, *J. Geophys. Res.*, **120**, 6320-6331 (2015)

Zaqarashvili, T.V., I. Zhelyazkov, L. Ofman: Stability of rotating magnetized jets in the Solar atmosphere. I. Kelvin-Helmholtz instability, *Astrophys. J.*, **813**, 123 (2015)

Zaqarashvili, T.V., R. Oliver, A. Hanslmeier, M. Carbonell, J.L. Ballester, T. Gachechiladze, I.G. Usoskin: Long-term variation in the Sun's activity caused by magnetic Rossby waves in the tachocline, *Astrophys. J. Lett.*, **805**, L14 (2015)

Zhang, L.Q., A.T.Y. Lui, W. Baumjohann, J.Y. Wang: Probabilities of magnetic reconnection encounter at different activity levels in the Earth's magnetotail, *Adv. Space Res.*, **56**, 736-741 (2015)

Zhang, L.Q., J.Y. Wang, W. Baumjohann, H. Rème, L. Dai, M.W. Dunlop, T. Chen, Y. Huang: X lines in the magnetotail for southward and northward IMF conditions, *J. Geophys. Res.*, **120**, 7764-7773 (2015)

Zhang, L.Q., J.Y. Wang, W. Baumjohann, H. Rème, M.W. Dunlop: Earthward and tailward flows in the plasma sheet, *J. Geophys. Res.*, **120**, 4487-4495 (2015)

Zhang, L.Q., L. Dai, W. Baumjohann, H. Rème, M.W. Dunlop, X.H. Wei: Parallel-dominant and perpendicular-dominant components of the fast bulk flow: Comparing with the PSBL beams, *J. Geophys. Res.*, **120**, 9500-9512 (2015)

Zhang, L.Q., W. Baumjohann, J.Y. Wang, H. Rème, M.W. Dunlop, T. Chen: Statistical characteristics of slow earthward and tailward flows in the plasma sheet, *J. Geophys. Res.*, **120**, 6199-6206 (2015)

Zhang, T.L., W. Baumjohann, C.T. Russell, M.N. Villarreal, J.G. Luhmann, W.L. Teh: A statistical study of the low-altitude ionospheric magnetic fields over the north pole of Venus, *J. Geophys. Res.*, **120**, 6218-6229 (2015)

Zhelyazkov, I., T.V. Zaqarashvili, R. Chandra: Kelvin-Helmholtz instability in coronal mass ejecta in the lower corona, *Astron. Astrophys.*, **574**, A55 (2015)

Zhelyazkov, I., T.V. Zaqarashvili, R. Chandra, A.K. Srivastava, T. Mishonov: Kelvin-Helmholtz instability in solar cool surges, *Adv. Space Res.*, **56**, 2727-2737 (2015)

BOOKS

Lammer, H., M.L. Khodachenko (Eds.): Characterizing Stellar and Exoplanetary Environments, Springer, Berlin, 310 pages (2015)

PROCEEDINGS & BOOK CHAPTERS

Alexeev, I.I., M.S. Grygoryan, E.S. Belenkaya, V.V. Kalegaev, M.L. Khodachenko: Magnetosphere environment from solar system planets/moons to exoplanets. In: *Characterizing Stellar and Exoplanetary Environments*, Eds. Lammer, H., M.L. Khodachen-ko, Springer, Berlin, 59-80, (2015)

Baumjohann, W., R. Nakamura: Magnetospheric Contributions to the Terrestrial Magnetic Field. In: *Treatise on Geophysics. Vol. 5: Geomagnetism (2nd Ed.)*, Ed. Schubert, G., Elsevier, Oxford, 79-90 (2015)

Belenkaya, E.S., M.L. Khodachenko, I.I. Alexeev: Alfvén radius: A key parameter for astrophysical magnetospheres. In: *Characterizing Stellar and Exoplanetary Environments*, Eds. Lammer, H., M.L. Khodachenko, Springer, Berlin, 239-246 (2015)

Bruyninx, C., A. Araszkiewicz, E. Brockmann, A. Kenyeres, R. Pacione, W. Söhne, G. Stangl, K. Szafranek, C. Völksen: EPN Regional Network Associate Analysis Center Technical Report 2014. In: *International GNSS Service Technical Report 2014*, Eds. Jena, Y., R. Dach, Astronomical Institute, University of Bern, Bern, 89-100 (2015)

Cheng, B., B. Zhou, W. Magnes, R. Lammegger, A. Pollinger, M. Ellmeier, C. Hagen, I. Jernej: Performance of the engineering model of the CSES high precision magnetometer. In: *IEEE Sensors 2015 Proceedings*, IEEE, Piscataway, 1933-1936 (2015)

Eastwood, J.P., S.A. Kiehas: Origin and evolution of plasmoids and flux ropes in the magnetotails of Earth and Mars. In: *Magnetotails in the Solar System*, Eds. Keiling, A., C.M. Jackman, P.A. Delamere, American Geophysical Union, Washington, D.C., 269-287 (2015)

Fischer, G.: Im Kontext: Blitze am Saturn. In: *Physik für Wissenschaftler und Ingenieure (7. Aufl.)*, Ed. Tipler, P.A. , G. Mosca, J. Wagner, Springer, Berlin, 752-753 (2015)

Fossati, L., C.A. Haswell, J.L. Linsky, K.G. Kislyakova: Observations of exoplanet atmospheres and surrounding environments. In: *Characterizing Stellar and Exoplanetary Environments*, Eds. Lammer, H., M.L. Khodachenko, Springer, Berlin, 59-80 (2015)

Khodachenko, M.L., and "Pathways to Habitability" Team: Stellar activity and CMEs: Important factors of planetary evolution. In: *Solar Prominences*, Eds. Vial, J.-C., O. Engvold, Springer, Heidelberg, 455-482 (2015)

Kislyakova, K.G., M. Holmström, H. Lammer, N.V. Erkaev: Stellar driven evolution of hydrogen-dominated atmospheres from Earth-like to super-Earth-type exoplanets. In: *Characterizing Stellar and Exoplanetary Environments*, Eds. Lammer, H., M.L. Khodachenko, Springer, Berlin, 137-151 (2015)

Maier, A., O. Baur: Sensitivity of simulated LRO tracking data to the Lunar gravity field. In: *Gravity, Geoid and Height Systems. IAG Symposium 141*, Ed. Marti, U., Springer, Cham, 337-342 (2015)

Mandt, K.E., J.L. Burch, C. Carr, A.I. Eriksson, K.-H. Glassmeier, J.-P. Lebreton, H. Nilsson, C. Béghin, T.W. Broiles, G. Clark, E. Cupido, N. Edberg, M. Galand, R. Goldstein, P. Henri, C. Koenders, P. Mokashi, Z. Nemeth, C. Pollock, I. Richter, M. Samara, K. Szego, C. Vallat, X. Vallières, M. Volwerk, G.S. Wieser, D. Winterhalter: First results at 67P/Churyumov-Gerasimenko with the Rosetta Plasma Consortium. In: *46th Lunar and Planetary Science Conference*, Lunar and Planetary Institute, Houston, 2312 (2015)

Mitterschiffthaler, P., D. Ruess, G. Stangl, H. Titz, Ch. Ullrich, E. Zahn: EUREF 15: National report of Austria. In: *Report on the Symposium of the IAG Subcommission for Europe (EUREF)*, EUREF, Leipzig, 4 p. (2015)

Narita, Y.: Turbulence reconnection in astrophysical plasmas and quantum fluids. In: *Proceedings of the 15th European Turbulence Conference*, Ed. TU Delft, TU Delft, Delft, No. 53 (2015)

Narita, Y.: Turbulent reconnection in astrophysical plasmas and quantum fluids. In: *Proceedings of the 15th European Turbulence Conference*, Ed. European Mechanics Society, European Mechanics Society, Delft, 53-54 (2015)

Reubelt, T., O. Baur, M. Weigelt, M. Roth, N. Sneeuw: GOCE long-wavelength gravity field recovery from 1s-sampled kinematic orbits using the acceleration approach. In: *Gravity, Geoid and Height Systems. IAG Symposium 141*, Ed. Marti, U., Springer, Cham, 21-26 (2015)

For oral presentations and posters please refer to www.iwf.oeaw.ac.at/en/publications.

PERSONNEL

Alexandrova, Alexandra, MSc
Almer, Hannes
Al-Ubaidi, Tarek, Dipl.-Ing.
Amerstorfer, Ute, Dr.
Andriopoulou, Maria, Dr.
Arkhypov, Oleksiy, Dr.
Aydogar, Özer, Dipl.-Ing.
Baumjohann, Wolfgang, Prof.
Baur, Oliver, Dr.
Bentley, Mark, Dr.
Berghofer, Gerhard, Ing.
Besser, Bruno P., Dr.
Boudjada, Mohammed Y., Dr.
Bourdin, Philippe, Dr.
Cubillos, Patricio, MSc
Delva, Magda, Dr.
Dwivedi, Navin, Dr.
Eichelberger, Hans U., Dipl.-Ing.
Fischer, David, Dipl.-Ing.
Fossati, Luca, Dr.
Fremuth, Gerhard, Dipl.-Ing.
Giner, Franz, Dipl.-Ing.
Graf, Christian, Ing.
Grill, Claudia
Hagen, Christian, Dipl.-Ing.
Hasiba, Johann, Dipl.-Ing.
Hofmann, Karl, Dipl.-Ing.
Höck, Eduard, Dipl.-Ing.
Hradecky, Doris
Jernej, Irmgard, Ing.
Jeszenszky, Harald, Dipl.-Ing.
Jurisiv, Mirjana
Juvan, Ines, Mag.
Kahr, Nina
Kargl, Günter, Dr.
Khodachenko, Maxim L., Dr.
Kiehas, Stefan, Dr.
Kirchner, Georg, Dr.
Kislyakova, Kristina, Dr.
Koidl, Franz, Ing.
Kömle, Norbert I., Doz.
Krauss, Sandro, Dr.
Kubicka, Manuel
Kürbisch, Christoph, Ing.
Laky, Gunter, Dipl.-Ing.
Lammer, Helmut, Dr.
Lechner, Lukas
Leichtfried, Mario, Ing.
Leitner, Stefan, Dipl.-Ing.
Lendl, Monika, Dr.
Lhotka, Christoph, Dr.
Lichtenegger, Herbert I.M., Dr.
Lopera, José Romero
Macher, Wolfgang, Dr.
Magnes, Werner, Dr.
Močnik, Karl, Dr.
Möstl, Christian, Dr.
Nakamura, Rumi, Doz.
Nakamura, Takuma, Dr.
Narita, Yasuhito, Doz.
Neukirchner, Sonja, Ing.
Nischelwitzer-Fennes, Ute, Ing.
Odert, Petra, Mag.
Ottacher, Harald, Dipl.-Ing.
Panchenko, Mykhaylo, Dr.
Panov, Evgeny, Dr.
Pitterle, Martin
Plaschke, Ferdinand, Dr.
Poganski, Joshua
Pollinger, Andreas, Dr.
Prattes, Gustav, Dipl.-Ing.
Reimond, Stefan, Dipl.-Ing.
Rollett, Tanja, Dr.
Sasunov, Jury, Dr.
Scherf, Manuel, Mag.
Scherr, Alexandra, Mag.
Schmid, Daniel, Dipl.-Ing.
Schmied, Roland
Schwarzbauer, Gerald
Shergelashvili, Bidzina, Dr.
Stachel, Manfred, Dipl.-Ing.
Stangl, Günter, Dr. (BEV)
Steinberger, Michael, Dipl.-Ing.
Steindorfer, Michael, Dr.
Steller, Manfred B., Dr.
Stieninger, Reinhard, Ing.
Tiefenbacher, Patrick, Mag.
Törmänen, Olli Juhani
Tschachler, Elvira, Mag.
Valavanoglou, Aris, Dipl.-Ing.
Varsani, Ali, Dr.
Voller, Wolfgang G., Mag.
Volwerk, Martin, Dr.
Vörös, Zoltán, Dr.
Wallner, Robert, Ing.
Wang, Peiyuan, Dr.
Wirnsberger, Harald, Dipl.-Ing.
Zehetleitner, Sigrid, Mag.
Zhang, Tie-Long, Prof.

As of 31 December 2015

BEV: Federal Office for Metrology and Surveying

IMPRESSUM

PUBLISHER

Wolfgang Baumjohann, Director
Institut für Weltraumforschung (IWF)
Österreichische Akademie der Wissenschaften (ÖAW)
Schmiedlstraße 6, 8042 Graz, Austria
iwf.oeaw.ac.at

EDITORS

Bruno Besser, Alexandra Scherr, Martin Volwerk

DESIGN

Alexandra Scherr
pr.iwf@oeaw.ac.at, @IWF_Graz

ÖAW

WWW.OEAW.AC.AT